Beyond the margins: real-time detection of cancer using targeted fluorophores

Ray R. Zhang[1,2,*], **Alexandra B. Schroeder**[3,4,5,*], **Joseph J. Grudzinski**[5], **Eben L. Rosenthal**[6], **Jason M. Warram**[7], **Anatoly N. Pinchuk**[1], **Kevin W. Eliceiri**[3,4,5,8,‡], **John S. Kuo**[2,8,‡], and **Jamey P. Weichert**[1,5,8,‡]

[1]Department of Radiology, University of Wisconsin–Madison (UW-Madison)

[2]Department of Neurological Surgery, UW-Madison, 600 Highland Avenue, Madison, Wisconsin 53792, USA

[3]Medical Engineering, Morgridge Institute for Research, 330 North Orchard Street, Madison, Wisconsin 53715, USA

[4]Laboratory for Optical and Computational Instrumentation, 1675 Observatory Drive, Madison Wisconsin 53706, USA

[5]Department of Medical Physics, UW-Madison, 1111 Highland Avenue, Madison, Wisconsin 53705, USA

[6]Department of Otolaryngology, Stanford Cancer Center, 875 Blake Wilbur Drive, Stanford, California 94305, USA

[7]Department of Otolaryngology, University of Alabama at Birmingham, 1670 University Boulevard, Birmingham, Alabama 35294, USA

[8]Carbone Cancer Center, UW-Madison, 600 Highland Avenue Madison, Wisconsin 53792, USA

Abstract

Over the past two decades, synergistic innovations in imaging technology have resulted in a revolution in which a range of biomedical applications are now benefiting from fluorescence imaging. Specifically, advances in fluorophore chemistry and imaging hardware, and the identification of targetable biomarkers have now positioned intraoperative fluorescence as a highly

Correspondence to J.P.W. JWeichert@uwhealth.org.
*Equal contributions were made by these two authors.
‡Equal contributions were made by these three authors.

specific real-time detection modality for surgeons in oncology. In particular, the deeper tissue penetration and limited autofluorescence of near-infrared (NIR) fluorescence imaging improves the translational potential of this modality over visible-light fluorescence imaging. Rapid developments in fluorophores with improved characteristics, detection instrumentation, and targeting strategies led to the clinical testing in the early 2010s of the first targeted NIR fluorophores for intraoperative cancer detection. The foundations for the advances that underline this technology continue to be nurtured by the multidisciplinary collaboration of chemists, biologists, engineers, and clinicians. In this Review, we highlight the latest developments in NIR fluorophores, cancer-targeting strategies, and detection instrumentation for intraoperative cancer detection, and consider the unique challenges associated with their effective application in clinical settings.

The developments in molecular imaging over the past two decades have revolutionized the field of biological imaging, with ongoing profound effects on research in life sciences. Subcellular structures and dynamic biological processes that were once optically indistinguishable from one another can now be visualized in great detail using fluorescence imaging against a background of complex cellular structures and homeostatic mechanisms, with a spatial and temporal resolution far superior to that obtained with conventional imaging modalities[1,2]. This approach is also poised to transform surgery.

Over the past few years, research efforts to develop targeted fluorophores for cancer imaging, coupled with the emergence of improved devices for fluorescence detection are set to revolutionize the field of oncological surgery. Surgery remains the cornerstone of treatment for solid tumours, but surgical techniques have not substantially changed over the past century. Surgeons rely on subjective assessments during resection (for example, of subtle tactile and visual tissue differences) to distinguish cancer tissues from the adjacent tissues intraoperatively, potentially resulting in either subtotal tumour resection or unwarranted removal of noncancerous tissue[3,4]. The presence of residual tumour tissue (defined as 'positive margins') after surgery has been reported in up to 30% of radical prostatectomies[5,6], 40% of pancreaticoduodenectomies[7], and 65% of high-grade glioma resections (in studies carried out in North America and Europe), highlighting the need for better intraoperative detection of malignant tissues[8,9]. While positive margins are associated with increased rates of local recurrence and worse clinical outcomes compared with complete resection[6,8,10–14], overzealous resection can remove or compromise adjacent vital tissue and organs, resulting in poor functional outcomes. With the use of fluorescence-guided surgery (FGS), malignancies that once evaded easy detection can be illuminated in real-time in the operating room. Robust detection of cancer tissue, directed by sensitive and specific tumour biomarkers, will eliminate reliance on nonspecific visual cues and tactile differences to distinguish malignant from benign tissues. Importantly, this diagnostic imaging modality could be used directly as a therapeutic aid for improving resection outcomes and thus, overall survival rates. Such an approach could also simultaneously decrease the rates of surgery-related co-morbidities, and improve functional outcomes by avoiding critical structures and preventing the need for repeated surgeries, and by reducing operating times and patient exposure to anaesthesia.

Fluorescence-guided imaging requires the administration of a cancer-selective exogenous fluorophore and imaging at the optimal time-point to achieve the best signal-to-noise contrast. Fluorophores with excitation and emission spectra in the near-infrared (NIR) wavelength range (700–900 nm) have attracted the most attention owing to their improved depth-penetration range compared with fluorophores that emit electromagnetic radiation of shorter wavelengths. *In vivo*, background fluorescence and scattering from water and chromophores are minimized in the NIR wavelength range[15,16] (FIG. 1). Cancer-targeted fluorophores have been widely explored in preclinical models, but only in the past 3 years have they been tested in clinical settings, with cetuximab-800CW being one of the first targeted NIR fluorophore to reach clinical trials[17]. The commercial development of these agents for clinical application has synergized with concurrent improvements in detection instrumentation and software.

Fluorescence imaging exhibits several favourable characteristics that are conducive for clinical translation, which include an excellent safety record with clinically-used probes[18–20], a lack of ionizing-radiation exposure, real-time detection capabilities with an adequate field of visualization (FOV), lower costs and much less cumbersome detection instrumentation compared with other intraoperative imaging modalities, and also provide a high sensitivity of detection[1,21–23]. Importantly, the ability to couple NIR fluorophores to target molecules in order to tailor fluorescence imaging for specific purposes enables the application of this modality to numerous clinical indications, especially in the field of oncology in which targetable biomarkers are now being characterized and validated in many cancer types[24]. Other imaging modalities, such as intraoperative CT and MRI, are not performed with targeted contrast agents as easily as NIR-based imaging because less-sensitive contrast agents are used[25]. In addition, introduction of expensive and bulky CT and/or MRI instrumentation in the surgical suite could also disrupt the surgical workflow.

For many decades, fluorescence has been used for the non-invasive detection of several physiological abnormalities. Fluorescein has been used since the 1960s for the diagnosis of various ophthalmic pathologies[26,27]. Vascular imaging with indocyanine green (ICG) has proven to be a cost-effective imaging modality in assessing perfusion of skin flaps after mastectomy[2,28,29]. Fluorophores have also been used for the detection of cancer, but only a small subset of tumour types can be detected using clinically approved nontargeted fluorophores[9,30].

Attaching fluorophores to targeting agents will enable the expansion of fluorescence imaging in clinical settings, and will improve the sensitivity and specificity of detection. The combination of improved NIR fluorophores with targetable cancer biomarkers has contributed to a surge of interest in fluorescence-guided surgery, evidenced by the introduction of NIR cancer-targeted fluorophores in clinical trials for the first time in the early 2010s (NCT01508572, NCT01987375). The cancer-targeted fluorophores used in clinical trials contain different fluorophores and leverage a spectrum of targeting strategies, including antibodies, small peptides, small molecules, activatable fluorophores, and multimodality fluorophores[31–35]. Herein, we discuss the latest advances in the development of fluorophores and instrumentation for performing FGS in the NIR range, with a particular

focus on the cancer-targeting strategies used and the regulatory challenges associated with the clinical adoption of this technique.

Approved fluorophores for cancer imaging

Indocyanine green

ICG is a heptamethine cyanine fluorophore, and is the first and only clinically approved fluorophore that displays NIR fluorescence[15]. The commercially available instrumentation used for ICG detection is adjusted for the characteristics that ICG displays in plasma (peak excitation wavelength of 807 nm, and peak emission wavelength of 822 nm)[36,37] (TABLE 1). IGC is hydrophobic and, thus, is frequently bound to proteins in plasma, which confines ICG to the intravascular space and makes it especially suited for angiography applications[38,39]. ICG-based angiography and lymphography have been used in a variety of clinical indications, such as perfusion-based imaging of the liver and blood vessels of the eye, and assessment of lymphatic vessel drainage[2,28].

Identification of sentinel lymph nodes (SLN mapping), and pathological assessment of lymph-node metastases offers important prognostic information for patients with breast cancer or melanoma[40]. To date, visible dye and radioscintography have been used for SLN mapping[40]. These two techniques are complementary — radionuclides provide information on the regional localization of primary lymph nodes, but the poor spatial resolution and the shine-through effect of radioscintography limits precise intraoperative mapping of SLNs, which can be achieved with optical imaging[21,40]. In the past few years, studies on SLN mapping have demonstrated enhanced detection sensitivity and specificity of ICG compared with blue dye and radioscintograpy[41–44]. The combined use of radioscintography and ICG has attracted interest because it enables preoperative planning before performing intraoperative biopsy[45–48].

ICG has also been used for intraoperative identification of liver metastases[49] and hepatocellular carcinomas[50–52] owing to the hydrophobicity and natural clearance of this fluorophore via the hepatobiliary system. In addition, because of having high plasma-protein-binding properties, ICG can extravasate passively into tumour tissues, which typically have a leaky vasculature and impaired lymphatic drainage[53]. This phenomenon, called the 'enhanced permeability and retention' (EPR) effect, has been used to nonspecifically detect cancers, including ovarian cancer and metastases[53], pancreatic cancer[54] or peritoneal metastases[55], among others. The use of passive targeting mechanisms, however, might not be ideal for specific detection, owing to reliance on low-contrast and nonspecific signals (for example, related to inflammation).

5-aminolevulinic acid

5-aminolevulinic acid (5-ALA) is an amino acid currently approved in Europe, Canada, and Japan for use in FGS of glioblastoma based on the results of a phase III clinical trial[9]. In cells with high metabolic activity, 5-ALA is processed via the haeme-synthesis pathway to produce abundant protoporphyrin IX, which exhibits a fluorescence absorption peak of 405 nm, and an emission peak in the red visible light range (635 nm), permitting fluorescence

imaging on the surface of tissues and in a depth-range of millimetres[56]. In addition, porphyrins have photodynamic properties and can generate triplet oxygen species when excited by light of appropriate wavelength (405 nm)[57]. These properties have been applied in the intraoperative treatment of cancers and premalignant lesions[9,57–59].

Studies have demonstrated that patients with gross total resections of both low-grade and high-grade gliomas have improved survival rates when compared with patients with subtotal resections[8,13,14]. In a European phase III clinical trial performed by Stummer *et al.*[9], patients who underwent FGS with 20 mg/kg bodyweight of 5-ALA ($n = 161$) had significantly improved total resection (65% versus 36%; $P < 0.0001$) and 6-month progression-free survival (41% versus 21%; $P = 0.0003$) rates than patients who underwent conventional microsurgery under white light ($n = 161$). The initial success with 5-ALA has spawned the initiation of clinical trials at academic centres outside Europe for fluorescent detection of gliomas (NCT01502280, NCT02119338, NCT02050243, NCT02191488).

5-ALA has also been used in clinical settings for the photodynamic detection and photodynamic therapy of many superficial skin lesions, and its use is being investigated in several cancer types[59–65]. 5-ALA is a small lipophilic zwitterion, and therefore the cellular penetration into lesions thicker than 2 mm decreases treatment efficacy[61,66–68]. In addition, the low tissue penetration of the protoporphyrin IX excitation and emission wavelengths limits the effectiveness of photodynamic therapy[61,66].

Methylene blue

Methylene blue is a clinically approved dye with visible and NIR fluorescent properties, and a unique biodistribution profile that has been exploited for cancer imaging. Methylene blue is commonly used as a blue dye in conjunction with radiocolloids to identify SLNs in patients with melanoma or breast cancer[28,40,47]. This agent exists in the form of several cations in solution and displays far-red fluorescence at low concentrations, with a peak emission wavelength of 688 nm[67,68]. The unique biodistribution and fluorescence properties of methylene blue have been exploited by several investigators to identify vital structures, including the ureters[69] and the parathyroid gland[71–73] (NCT02089542, NCT01598727), as well as cancers such as neuroendocrine insulinomas[74], fibrous pancreatic tumours[75], paragangliomas[30], and para thyroid adenomas[72], albeit in small case studies; however, the tumour targeting properties of methylene blue remain poorly understood. Methylene blue also exhibits photodynamic properties, with a high efficiency of generating triplet oxygen species when excited by light[76]. Photodynamic treatment of blood-borne infections[71,77,78] (NCT00917202), and sepsis (NCT01797978) with methylene blue has been reported.

Fluorophore development

Although ICG, 5-ALA, and methylene blue have been investigated in nontargeted applications[2], their use in oncological imaging has been limited by several key factors, including the lack of specific cancer-targeting and conjugation potential of ICG, the limited knowledge of the tumour-targeting potential of methylene blue, and the poor tissue penetration and imaging depth properties of 5-ALA. Thus, research efforts of the past decade have focused on developing new NIR fluorophores with improved tissue-depth

penetration, and then transforming them into cancer-selective fluorophores. Remarkable improvements in the photophysical and photostability properties of organic fluorophores have made them suitable for *in vivo* applications; these organic fluorophores now display fluorescence in the NIR window (700–900 nm). Properties such as tissue absorbance, autofluorescence, and light scattering are improved in this range compared with the visible light range, and thus, signal-to-noise ratio (SNR) and depth of detection (up to 1 cm) are enhanced[15,79,80] (FIG. 1). Substantial absorbance is detected below this window, by chromophores and water.

To be used *in vivo*, fluorophores should demonstrate fluorescence in the NIR window, and should also have good solubility, photophysical characteristics (brightness, and peak excitation and emission wavelengths (Stokes shift), and photostability. Owing to their hydrophobicity, fluorophores often demonstrate poor solubility and aggregation in solution, which can lead to changes in their excitation and emission ranges, as well as quenching of fluorescence[38,39]. Fluorophores should also demonstrate optimal photophysical characteristics, including brightness; molar absorptivity (ϵ), a product of how well they absorb excitation photons; and fluorescence quantum yield (Φ), which indicates how often that absorbance leads to emission of fluorescence. Moreover, their Stokes shift should be sufficient (>30 nm) to enable ease of detection, otherwise light contamination and decreased sensitivity can pose concern. Photostability is a general term that describes the retention of the photophysical properties in different chemical environments; to enable accurate assessment, fluorophores should demonstrate photostability *in vivo*, especially considering that detection cameras have different sensitivities at different wavelength ranges. Common photostability concerns with fluorophores include photobleaching, changes in the photophysical characteristics in different media, and changes in photophysical characteristics after plasma-protein-binding or conjugation to a targeting ligand[81,82]. Lastly, conjugatable fluorophores should be available for targeted probe development.

Cyanine fluorophores

Cyanine fluorophores have remained the most popular fluorophores for conjugation with targeted ligands owing to their favourable safety profiles, tunable fluorescence characteristics, good solubility, and the commercial availability of conjugates[81]. ICG and IRDye® 800CW (IR-800CW; Li-COR Lincoln, Nebraska, USA) are cyanine fluorophores that have undergone safety testing by the FDA. Indeed, ICG has an excellent safety record in clinical settings[18,20]. IR-800CW has undergone a microdosing study meeting the requirements for an FDA exploratory Investigational New Drug study (IND, also referred to as phase 0), with ICG used as control[19]. These molecules represent two of the most commercially developed fluorophores and, currently, IR-800CW conjugates are among the first targeted probes to be tested in several clinical trials for NIR imaging (TABLE 2).

Cyanines contain two aromatic nitrogen-containing heterocyclic ring systems linked by a polymethine bridge. Extension of the polymethine bridge increases the wavelength of emission and excitation, with trimethine (Cy3) and pentamethine (Cy5) fluorophores displaying fluor escence in the visible and far-red range, respectively, and heptamethine (Cy7) fluorophores displaying fluorescence in the NIR range[83]. ICG was the first NIR

fluorophore approved for imaging, but the suitability of this agent is limited because of its low fluorescence quantum yield[84], lack of conjugation potential[19], and poor *in vivo* photostability owing to plasma-protein binding, photobleaching and aggregation[39,85,86].

Many improvements in the optical properties of cyanine derivatives have been made since ICG was first developed. The introduction of a rigid cyclohexyl moiety in the middle of the polymethine bridge, of electron-donating groups on the *N*-substituent of the 3H-indolenine, and of a central chlorine atom on the cyclohexyl moiety have substantially improved the photostability and decreased aggregation of these agents[87,88]. The addition of sulfonic acid or carboxylic acid groups enhances the solubility, fluorescence intensity, and Stokes shift of these fluorophores[89]; IR-800CW is a novel cyanine fluorophore exhibiting these improved characteristics[19]. Choi *et al.*[90] developed ZW800-1, a zwitter ionic cyanine fluorophore with a net neutral surface charge, which displayed low plasma-protein binding affinity, improved *in vivo* photostability, decreased nonspecific uptake, as well as favourable pharmacokinetic (PK) and biodistribution characteristics[37,90].

Other fluorophores

Other fluorophore classes are less well-developed than cyanine fluorophores, but also display translational potential. In the past decade, efforts have focused on shifting fluorescence profiles to longer wavelengths, that is, from the visible light range to 700–900 nm (NIR I spectrum), and from the NIR I range to 1,000–1,700 nm (NIR II spectrum). Additional efforts to improve the photophysical and photostability characteristics of fluorophores have resulted in the preclinical development of fluorophores such as squaraines, BODIPY fluorophores, rhodamines, porphyrins, and pthalocyanines that now display fluorescence in the NIR window[81,83,91] (TABLE 2). Common strategies to shift the fluorescence spectra of these compounds have relied on extending the aromatic system and increasing molecular rigidity[81,91]. These modifications, however, are usually accompanied by increased hydrophobicity, which results in poor solubility in water, nonspecific binding, and slow biological clearance[37,91]. Ongoing efforts are focused on improving the solubility of these fluorophores in order to render them more suitable for *in vivo* applications.

The encapsulation of these fluorophores can substantially enhance their solubility, photostability and photophysical characteristics. Conjugation with polyethelene glycol (PEGylation) has been used to increase the solubility of these hydrophobic fluorophores and improve their PK properties[32,81,92]. Antaris *et al.*[92] described CH0155, the first small-molecule organic fluorophore with excitation and emission spectra in the NIR II window with favourable water solubility and fast biological clearance achieved through PEGylation. When used for imaging, PEGylated fluorophores demonstrated improved spatial resolution in the vasculature and lymphatic system compared with ICG (in the NIR I range)[92]. In addition, PEGylated fluorophores conjugated with a targeting ligand showed a fivefold increase in tumour-to-background signal compared with an NIR I fluorophore conjugated with the same targeting ligand[92,93]. LUM015, an activatable fluorophore tested in clinical trials for the detection of soft-tissue sarcoma and breast cancer also incorporates PEGylation to achieve improved PK properties[32]. Thus, the PEGylation of fluorophores represents a way

of overcoming their inherent hydrophobicity and poor PK properties while preserving their safety profile *in vivo*[32,92,94].

Other encapsulation methods, such as the use of nanoparticles, have been used in preclinical studies to deliver fluorophores to animals with cancer, while simultaneously maintaining their photophysical properties and photostability. Fluorophore targeting can involve passive mechanisms, such as EPR, whereby increased vascular permeability and/or decreased drainage of tumour vessels enable large molecules to accumulate within tumour tissue[53], or the incorporation of active targeting components on the surface of the nanoparticle. Owing to their protective encapsulation, nanoparticle-loaded fluorophores display excellent photophysical and photostability properties, including bright signals, low aggregation, and even tunable spectral properties[81,83]. Despite advances in the development of nanoparticle-loaded fluorophores, the toxicity of nanoparticles and manufacturing difficulties associated with them have hampered their application in translational studies[81,83].

Targeted fluorophore development

PK, biodistribution, and dosing

Targeted fluorophore development usually entails the conjugation of fluorophores to cancer-targeting agents through a linker. By using targeted fluorophores, the sensitivity and specificity of detection for disease-specific applications is increased, with favourable SNR profiles[95]. Currently, fluorophores have not been approved by the FDA for intraoperative cancer imaging; however, in the past few years, an increasing number of clinical trials have tested targeted fluorophores that leverage a variety of targeting strategies (FIG. 2).

The choice of target and fluorophore for a cancer-targeting fluorophore can affect its PK and biodistribution. Sufficient contrast and specificity are achieved when the ligand has a high affinity for a target highly expressed in a particular cancer type, which can be extracellular (such as receptors or enzymes), or intra cellular (such as intracellular enzymes). Many growth-factor receptors are overexpressed in cancer cells and can be targeted by a variety of ligands, such as antibodies, small antibody fragments, peptides, or even small molecules[24]. Antibodies are large (>100 nm), and therefore fluorophore–antibody conjugates exhibit long circulation times and nonspecific tumour uptake through the EPR effect[96–98]. Small targeting ligands exhibit faster PK properties, thus achieving sufficient contrast much quicker than large molecules, which enables imaging sooner after administration[99]. On the other hand, small targeting ligands are less amenable to conjugation and chemical modifications than large molecules, and small structural changes can drastically affect their targeting and PK properties[95,99].

Targeting extracellular enzymes can be a feasible approach to design activatable probes with high SNR. Cathepsins and matrix metalloproteinases (MMPs) are extracellular matrix enzymes overexpressed in numerous cancers. In cancer, as well as in inflammatory conditions, MMPs and cysteine cathepsins alter the microenvironment, facilitating invasion and metastasis[100–103]. Protease-activated probes generally consist of a quencher conjugated to a fluorophore through a cleavable linker that can be recognized by proteases commonly present at increased levels in the tumour microenvironment, resulting in increased activation

of fluorescence, than in nonmalignant tissues. The challenges associated with this approach are the diffusion of activatable fluorophores within the tumour microenvironment, and decreased specificity, owing to the roles in both cancer and inflammation of the enzymes used in activation[104–106]. For intracellular targets, the fluorophore–ligand conjugate must enter cancer cells either through passive diffusion or via active uptake of the target (exploiting ligands that specifically bind to cancer cells)[99]. High doses of fluorophore–ligand conjugates that passively diffuse into cancer cells might be required to achieve sufficient contrast[99].

The conjugation of a fluorophore to a targeting ligand might not only affect the photophysical and photostability properties of the cancer-targeted fluorophore, but also its PK and biodistribution properties[79,95]. As a general rule, the PK and biodistribution of the spatially larger group predominate. Linkers can be incorporated to potentiate interactions between the fluorophore and targeting ligand (which can minimize quenching of the fluorophore), as well as the targeting ligand and the binding site[82]. In addition, cleavable linkers are necessary for enzyme-activated targeted fluorophores, which are recognized by proteases resulting in the release and activation of the fluorophore at the target site[24,35,99].

PK properties affect the optimal imaging time point of targeted fluorophores. Because large ligand-fluorophore conjugates (>100 nm) and hydrophobic conjugates bind to plasma proteins and are slowly cleared by the body, delays (hours to days) can occur between administration of the targeted fluorophore and the time of imaging. Targeted fluorophores should be designed with favourable PK properties tailored for their clinical use. An ideal targeted fluorophore should exhibit rapid tumour uptake and prolonged retention of the targeted fluorophore, as long as the targeted fluorophore is eventually cleared, or is nontoxic[104].

Similarly, the biodistribution properties inform on the usefulness of these targeted fluorophores, because this parameter describes which nonmalignant organs have a role in excretion and nonspecific binding[2,15,53]. A combination of high binding affinity for cancer tissue with minimal nonspecific organ binding is ideal, but often not achieved. As the ligand, linker, and fluorophore can affect biodistribution, the individual contribution of each component might be hard to predict and, therefore, new targeted fluorophores should undergo testing *in vivo.*

Using smaller antibody fragments[98,107,108], employing pretargeting strategies and paired probe methods[25,109,110], and combining activation and targeting strategies[79] can decrease circulation times, increase the specificity of targeted fluorophores, and lead to more-favourable biodistribution, thus decreasing potential associated toxicities. The limitations of these strategies and ongoing improvements have been discussed in detail elsewhere[35,79,99].

Lastly, another important parameter that influences PK and safety profiles is dosing. Dose-escalation studies are designed to determine the maximum tolerated dose and determine if an effective dose is safe[111,112]. Preclinical studies can help determine the PK profiles and appropriate dosing of targeted fluorophores — scaling up the dose in experiments with other mammalian species and in studies with humans according to body surface area can give a

good initial estimate for the appropriate dose[111]. Pilot clinical trials, and phase I and II clinical studies will ultimately determine the appropriate dose and optimal imaging time point for these agents[112].

Ligand-targeted fluorophores

Conjugation of fluorophores to cancer-specific ligands increases the sensitivity and specificity for cancer cells that express the receptors for those ligands, enabling the use of low concentrations for fluorescence detection[79,104]. Cancer-specific ligands tested in clinical trials include antibodies, peptides, and small ligands (TABLE 3).

After the approval of the anti-CD20 monoclonal antibody rituximab in 2006, no less than 15 monoclonal antibodies have been approved for cancer therapy[113]. Importantly, once approved, these antibodies can be repurposed for diagnostic applications, such as FGS. Bevacizumab-800CW, a monoclonal antibody to VEGF, is being evaluated for the diagnosis of a variety of premalignant and malignant conditions, including colorectal cancers[11] (NCT01508572, NCT02583568, NCT02129933, NCT01972373, NCT01691391). Previous studies performed on human colorectal biopsy specimens have identified VEGF as a promising target with 79–96% ($n = 304$) of colorectal lesions expressing VEGF-A[114]. More than 95% of head and neck squamous-cell carcinomas overexpress EGFR and thus, cetuximab-800CW and panitumumab-800CW, both targeting EGFR, are undergoing evaluation for intra operative detection of these tumours[115,116] (NCT01987375, NCT02415881; FIG. 3). huJ591 is a second-generation antibody that targets prostate-specific membrane antigen (PSMA), which is highly expressed in virtually all prostate cancers[117,118]. Bander *et al.*[119] demonstrated in preliminary clinical trials that a radioconjugate form of huJ591 had a sensitivity of nearly 100% for the identification of soft-tissue and bone metastases in patients with prostate cancer; huJ591 is now being conjugated to IR800-CW for the intraoperative detection of residual disease in such patients (NCT01173146). Up to 30% of prostatectomies leave residual tumour, and therefore the clinical need to identify residual disease intra operatively remains to be addressed[5,120]. Other antibody–fluorophore conjugates are in preclinical development, including some featuring both approved antibodies (daclizumab, trastuzumab, and panitumumab) and the approved fluorophore ICG[82,94,121]. Recognized limitations of antibody-based imaging include poor extravasation into the tumour (owing to large molecular size), long circulating half-life, and nonspecific uptake through the EPR effect[96–98]. Ongoing efforts to decrease the circulation times using smaller antibody fragments[98,107], and pretargeting strategies[109,110] are at the preclinical stage.

BLZ-100 is an imaging agent composed of a small-peptide chlorotoxin, which targets annexin A2, conjugated to functionalized ICG[31]. Annexin A2 overexpression has been exploited to label many solid tumours, including primary brain tumours and other neuroectodermal tumour types, and is now being evaluated clinically in several phase I trials after successful proof-of-concept trials in canine cancer models[31,122–124] (NCT02496065, NCT02464332, NCT02462629, NCT02234297). A small-peptide, cyanine fluorophore conjugate, GE-137, was developed for endoscopic detection of hyperplastic and malignant polyps that overexpressed MET (also known as hepatocyte growth factor receptor)[125,126].

Burggraaf *et al.*[125] designed a Cy5-fluorophore conjugated to a peptide with high-affinity for an extracellular epitope of MET that displayed fast PK properties and a favourable safety profile in healthy human volunteers, and performed imaging with a prototype endoscope optimized for GE-137. In a sample cohort with 15 patients harbouring a total of 101 polyps, these agents enabled visualization of all neoplastic polyps that were visible under white light, in addition to 9 polyps that were not visible in those conditions[125].

Many cancers, including carcinomas of the breast, lung, and ovary, express high levels of folate receptor (FR)-α[127]. Van Dam *et al.*[33] performed an initial clinical pilot study with EC17, a conjugate comprising fluorescein isothiocyanate and the small molecule folate. Sensitive and specific intraoperative detection of FR-α-positive ovarian cancer with this targeted conjugate was demonstrated in a study involving 12 patients with ovarian cancer[33]. This agent is being further evaluated in phase I trials in patients with lung, breast[128], or renal cancers, in which this agent shows promise in detecting metastases owing to a high rate of concordant expression of FR-α between the primary cancer and metastases[129] (NCT01996072, NCT01994369, NCT01778933, NCT01778920, NCT02317705). EC17 is also being evaluated in phase I trials for the detection of primary hyperparathyroidism. OTL38, a folate–Cy7-fluorophore conjugate with good depth penetration, is being evaluated for the intraoperative detection of FR-α-positive ovarian cancer (NCT02317705)[99]. In 2015, a comparison of OTL38 and EC17 demonstrated that OTL3 exhibits a 3.3-fold higher signal-to-background ratio in mouse-flank tumour xenografts, and very minimal autofluorescence compared with EC17, illustrating the advantages of NIR fluorescence over visible-light fluorescence[34].

We have developed small-molecule alkylphosphocholine (APC) analogues that display avidity for a wide array of cancers including glioblastoma, breast, and colorectal cancers[130–133]. These small molecules are selectively taken up in lipid rafts, which are abundant on cancer cells and cancer-stem cells, and are subsequently retained in cancer cells owing to a deficiency of catabolic enzymes[130]. CLR1502, a conjugate of the fluorophore IR-775 with APC, can potentially be used for intraoperative detection of numerous cancer types in clinical settings[131–133] (Supplementary information S1 (movie)). CLR1502 demonstrated an impressive SNR in orthotopic mouse models of human glioblastoma, with an average SNR of 9.3 and a twofold greater SNR compared with 5-ALA-based imaging[133]. Use of this targeted fluorophore can substantially improve resection outcomes in GBM, in which only around 35% of surgeries result in clear margins[8,9]. Delineation between malignant and benign tissues is especially important in GBMs owing to the vital importance of avoiding damage to adjacent nonmalignant brain tissue, and to the high recurrence rates in these aggressive cancers. Importantly, these APC analogues can be used for multimodality imaging and therapeutic applications because they exploit the same mechanism of uptake and retention as a suite of diagnostic imaging and targeted-therapy analogues (I-124-CLR1404 and I-131-CLR1404) currently in preclinical and clinical development[130,134–136] (NCT01898273, NCT00925275).

Activatable fluorophores

Fluorophores can be designed to emit fluorescence only after binding the target tissue, substantially enhancing the SNR by simultaneously decreasing the background and increasing the fluorescent signal activated upon target binding. Strategies in activated fluorophore design utilize photochemical quenching, ligand-targeted activation, or both[79,95]. Photochemical quenching methods rely on self-quenching, homofluorescence and heterofluorescence resonance energy transfer, H-dimer formation, and photon-induced electron transfer, which have been discussed in detail elsewhere[95].

The activatable fluorophores that have initially been tested in clinical trials include LUM015 and AVB-620, which leverage mechanisms of protease activation that we have already discussed. Whitley *et al.*[32] evaluated LUM015, the first activatable fluorophore to be tested in clinical trials, in a cohort of 15 patients with soft-tissue sarcoma or breast cancer (NCT01626066), after the initial success of preclinical studies in dogs and mice[32,137]. LUM015 is composed of the quencher QSY21 linked to a Cy5 fluorophore and a 20 kDa PEG molecule[32]. Upon cleavage of the linker by cathepsin, the Cy5 fluorophore becomes unquenched and can illuminate tumour margins. Initial studies demonstrated that LUM015 is selectively distributed to tumours, and its activation provides an average tumour-to-normal-tissue contrast ratio of 4.1 (REF. 32). The ratiometric activatable cell-penetrating peptide AVB-620, developed by the teams of Tsien and Nguyen[105,106], is undergoing initial clinical pilot studies in patients with breast cancer (NCT02391194). These activatable cell-penetrating peptides are composed of a polycationic peptide conjugated with Cy5 and Cy7 fluorophores, a cleavable linker, and a polyanionic fragment[115,116]. Upon cleavage of the linker by MMP-2 and/or MMP-9, the polycationic peptide and attached fluorescent cargo can penetrate into tumour cells and lymph-node metastases. Initially, the Cy5 fluorophore is quenched owing to the close proximity to Cy7 but, upon cleavage, the Cy5 signal to Cy7 signal ratio increases over 40-fold[106]. The use of ratiometric imaging circumvents the problems associated with quantification using single-wavelength intensity measurements (dose-dependent uptake and PK characteristics), and the fluorophore exhibits fast activation (within 2 h)[106,138,139].

Other fluorophores used preclinically, but with strong translational potential are in development. Urano, Kobayashi and colleagues[104] synthesized and tested γ-glutamyl hydroxymethyl rhodamine green (γ-Glu-HMRG) with intramolecular spirocyclic caging that resulted in complete quenching. Glutamate cleavage with γ-glutamyltranspeptidase (GGT), which is not expressed in normal tissue, but is overexpressed on the cell membrane of various cancer cells, including cervical and ovarian cancers, leads to the complete uncaging and unquenching of the fluorophore. In mouse models of disseminated human peritoneal ovarian cancer, activation of γ-Glu-HMRG occurred within minutes of spray-on application[104]. Nevertheless, problems associated with diffusion of such activatable fluorophores and nonspecific activation in an inflammatory milieu might decrease the specificity of detection[35,102,103]. In other studies, pH-activatable fluorophores, such as pH-activatable BODIPY[140] and cyanine fluorophores[141], have been used to visualize tumours.

Combination of activating and targeting strategies is currently being pursued in order to increase the specificity of activation[95]. In a preclinical study, ICG was conjugated to

clinically approved monoclonal antibodies (such as daclizumab, trastuzumab, and panitumumab), which quenched fluorescence through purported hydrophobic interactions between the fluorophore and antibody[82]; however, fluorescence was unquenched upon tumour uptake and dissociation of ICG from the antibody. The adoption of antibody–ICG conjugates in clinical settings might prove easier than that of other fluorophore-related compounds because both the fluorophore and the targeting antibodies are currently approved for clinical use, and clinical imaging devices optimized for ICG are readily available. Importantly, these conjugates display excellent signal-to-background ratios owing to the combined effect of targeting and activation.

Inherent-targeting naked fluorophores

Several fluorophores have been developed to have the inherent ability of targeting tumours. For example, Tan *et al.*[140] demonstrated cancer-selective uptake of the heptamethine cyanine fluorophore IR-780 in multiple rodent xenograft models of cancer and in a chemically-induced lung cancer model. Other Cy7 fluorophores, such as IR-783 and MH148, also target multiple cancer cell lines; IR-783 demonstrated good *in vivo* tumour uptake in rodent-flank xenograft models of human prostate, bladder, pancreatic, and renal cancers[141,142]. Tumour uptake and tumoricidal activities have also been described for derivatives of IR-783 and MH148, including IR-780 and IR-808 (REFS 142,145). In addition, Pz 247, a porphyrin analogue, exhibits selective uptake in subcutaneously implanted breast-cancer xenografts in mice[146]. The accumulation of lipophilic charged infrared fluorophores in tumours can be facilitated using organic cation transporter proteins, and organic anion transporter proteins (OATPs) owing to the high mitochondrial membrane potentials detected in malignant cells[143,147]. In 2014, Wu and collaborators[148] (NCT02464332) demonstrated that hypoxia upregulates the expression of OATPs, resulting in *in vivo* uptake of MH148 and average SNR values of 9.1. The ability of these fluorophores to target cancer might represent a feasible method leveraging small molecules, which might have the advantages of simplicity and low costs. The uptake of such small molecules might be further optimized through additional studies of structure–activity relationships.

ICG and methylene blue have both demonstrated structure-inherent targeting activity towards many cancer types and nonmalignant organs, possibly owing to OATP-mediated transport and to the EPR effect[30,49,72,75,149,150]. Many new fluorophores with structure-inherent targeting potential for other tissues are under development (for example, fluorophores that illuminate nerves[151,152], and the parathyroid and thyroid glands[153]); such fluorophores could prove useful in delineating vital organs and structures during surgery. As the detection technology and the arsenal of available fluorophores with different spectral properties continue to grow, multispectral imaging — that enables imaging of multiple organs of interest with cocktails of targeting fluorophores — will become a possibility[79]. Hyun *et al.*[153] have demonstrated proof-of-concept of multispectral imaging to distinguish the thyroid gland from the parathyroid gland during surgery using a cocktail of two targeted fluorophores and a dual-channel NIR imaging system. In addition, paired probe methods — using a targeted fluorophore and an untargeted fluorophore with different spectral properties — might help resolve the issue of nonspecific targeting[154].

Multimodality fluorophores

Each imaging modality has unique strengths and limitations and thus, combining multiple imaging modalities is a strategy to overcome the limitations of single modalities by synergizing the benefits of both modalities. Low depth of penetration and lack of robust quantification limit fluorescence detection, even in the NIR range. Combining fluorophores with radioactive tracers would integrate the advantages of quantitative detection and the unlimited depth of detection of radioactive tracers, and the high spatial resolution and functional molecular imaging potential of targeted fluorophores that are ideal for *in vivo* applications. SLN mapping using such a dual-modality approach has been initiated in human clinical trials for preoperative detection and intra operative illumination of many solid tumours[155]. The first clinical trial with a targeted multimodality single photon emission computed tomography (SPECT)/fluorophore imaging is underway[156]: indium-111-DOTA-girentuximab–IR-800CW is being evaluated as a dual-labelled agent for image-guided surgery (NCT024975599); girentuximab is a monoclonal antibody to carbonic anhydrase 9, which is expressed in 95% of renal-cell carcinomas[157]. Thus, the use of this agent might bridge preoperative detection and intra operative fluorescence detection of renal-cell carcinomas. In addition to preoperative staging and localization, the use of theranostic radiotracers can help characterize the PK properties, dosing, and quantification of their fluorescent counterparts; which otherwise might be difficult and invasive owing to the limited depth penetration of fluorescence.

The development of dual-modality probes with radiotracer and fluorescence modalities, and cocktails of theranostic companions can facilitate the clinical testing of fluorescent probes; however, the FDA does not permit testing two agents in a single clinical trial design and thus, the use of theranostic probes to facilitate the translation of fluorescent counterparts in the clinical setting will require the development of innovative strategies, new guidelines, or prior approval of theranostic radiolabelled probes. Indeed, many radioactive probes for cancer detection are currently under preclinical and clinical development, which holds promise for the use of theranostic radiotracers in conjunction with their fluorescent counterparts[119,121,158,159] (NCT01691391, NCT01894451).

Barriers to clinical adoption

Targeted fluorophores have the potential to change the way oncological surgeries are performed. Real-time sensitive and specific detection of cancer intraoperatively has the potential to improve survival outcomes for patients, as well as decrease the rate of comorbidities associated with prolonged exposure to anesthesia, repeat surgeries, and removal of normal functional tissues. For FGS to bear promise, however, several application, regulatory, and clinical challenges remain; some are characteristic of any new technology, whereas others are unique to fluorescence technologies. Herein, we outline the major challenges that currently impede the clinical adoption of FGS.

Application challenges

The detection of NIR fluorophores is constrained by the compatibility of the optimal detection instrumentation with the currently used surgical tools and setup of the operating

room. Importantly, the surgical workflow should be minimally affected to facilitate the adoption of this technology. Integration of the detection instrumentation with surgical tools has led to the development of a variety of devices for open-field surgery[33,160–162], endoscopes[23,163], and laparoscopes[164,165] for intraoperative NIR fluorescence visualization (TABLE 4). In addition to integrating camera systems, many of these devices superimpose the fluorescence image onto the surgical FOV to prevent alternating between two FOVs.

Special lighting conditions are also necessary in the operating room: during fluorescence visualization with both ICG and 5-ALA, the lighting must be dimmed or switched off to prevent light contamination[166,167]. To circumvent this problem, transient lighting approaches have been developed to switch from NIR collection to ambient lighting at a frequency sufficiently high enough to avoid disrupting the surgical workflow or markedly decreasing detection efficiency. Switching to light-emitting diode (LED) technology with NIR reflective films can also substantially decrease interference from NIR[168].

A learning-curve exists for the proper application of any new technology; as FGS becomes widespread, surgeons using this technology might require additional training to use the detection instrumentation and to be knowledgeable about the unique behaviour of targeted fluorophores, in order to ensure a safe and effective use of these agents[169].

Regulatory challenges

Successful pairing of camera specifications and fluorophore properties achieves the highest sensitivity for the minimal amount of fluorophore required for FGS. The FDA can require pairing of an optimized detection device to a particular fluorophore (termed a 'combination product') to approve clinical testing in conditions that facilitate appropriate use and mitigate toxicity[3] (FIG. 4). Currently, the only clinically approved instruments are optimized for the wavelength profile of ICG, and have not been optimized for the detection of low amounts of the fluorophore[170]. Newly developed fluorophores might have unique excitation and emission profiles that would not be compatible with this clinically approved instrumentation and thus, might need to be paired with a customized detection device tailored to their properties; some investigators have developed custom imaging systems tailored to the excitation and emission spectra of fluorophores they have designed[32,171]. Pairing devices to specific fluorophores, however, might be a restrictive approach that would impede the clinical adoption of FGS[1,3,21]. An alternative to individual fluorophore-device pairings would be to pair fluorophores with devices according to wavelength overlap[170].

In the USA, traditional drug-development pathways can be expensive and time-consuming. To date, ICG and IR800-CW are the only NIR fluorophores that have undergone safety testing[18,19]. Exploratory (e)IND studies could facilitate the preclinical-to-clinical translation of new targeted fluorophores, such as IR800-CW and several novel targeted fluorophores undergoing the same process[19] (NCT01173146, NCT02048150, NCT01778933). eINDs enable early clinical trials (phase 0) to proceed with a limited amount of clinical data (10–15 patients) if the investigational imaging agent is administered at subpharmaceutical doses (100 μg of a synthetic drug or 30 nmol of a protein)[171]. These studies can help investigators to determine the feasibility of using a targeted fluorophore in a very small number of patients before additional resources are spent on a more-traditional IND process.

The initial characterization of PK and pharmacodynamic parameters can be done in healthy volunteers, and dose-escalation studies designed according to novel model-based designs or specifically for molecularly targeted agents can be used in order to mitigate potential complications for patients with cancer and to encourage patient enrolment[25,112,125]. Other regulatory bodies, such as the European Medicines Agency, have different policies, but encounter similar challenges. At this early stage in FGS development, all the regulatory bodies are learning how to address the regulatory process for targeted fluorophores and devices; whether a fluorophore and companion device with clinical applicability will be regulated as a drug, device, or combination product remains an open question[3].

Clinical trial considerations

The agents discussed herein represent the adoption of new strategies for surgical resection — currently, no agreement exists on what the gold standard for clinical trial designs should be in order to demonstrate efficacy and safety of these approaches. Potential primary clinical end points are sensitivity and specificity of detection compared with histological confirmation, recurrence rates, and survival outcomes[34]. Secondary end points might include potential reduction in operation durations, associated costs, and rates of repeat surgeries and/or potential complications. These end points might need to be specific to the cancer type being evaluated. Moreover, the inability to blind the surgeons to FGS poses an additional challenge in clinical trial design. For multicentre studies, quantitative standards to compare detection sensitivities of different instruments are also needed.

The surgical approach and technique varies substantially between disease types and anatomical locations, which in turn influence the potential clinical value of FGS. Careful considerations of cancer types that can be favourably affected using FGS are warranted; not all cancers will benefit from FGS (for example, cancers with very high cure rates). Conversely, minimally invasive surgical techniques that occur in low ambient-light environments with limited tactile feedback in which the surgeon is operating from a monitor (such as laparoscopic surgery or robotic surgery) are likely to benefit from FGS[3,4].

In addition, studies in the patient groups most likely to benefit from FGS need to be undertaken. Candidates for FGS should exhibit expression of the targetable biomarkers; however, the heterogeneous expression patterns that exist between patients and even within the same patient can complicate the candidate selection process. Histological confirmation or preoperative staging with theranostic radiotracers might help identify candidates most likely to benefit from FGS[3,4]. Other challenges to the clinical adoption of FGS are discussed in further detail in a recent consensus report of the first International Society of Image-Guided Surgery meeting[3].

Conclusions

The *in vivo* use of NIR fluorophores has garnered increasing attention because of their favourable wavelength characteristics and ability to be conjugated to known tumour-targeting agents, enabling intraoperative cancer detection. Currently, surgeons must rely on nonspecific tactile and visual cues to distinguish tumours from adjacent nonmalignant tissues, and have at their disposal a few fluorophores with limited tumour-targeting potential

and unfavourable photophysical characteristics. In the past few years, multiple targeted fluorophores have been introduced in clinical trials; such agents feature targeted fluorophores with improved properties, and novel cancer-targeting strategies. With the development of fluorophores with improved physicochemical and tumour-targeting properties, and of new detection instrumentation, surgeons could soon achieve sensitive and specific intraoperative cancer detection. This advance could revolutionize the management of patients with cancer by improving the safety of surgical oncology procedures, increasing the efficiency and effectiveness of discrimination between cancers and vital structures, and decreasing the rates of surgery-related morbidities. Survival outcomes can be improved by real-time visualization of primary and metastatic tumours at and beyond the margins, which would maximize resection efficiency and improve cancer staging (for example, with SLN mapping). In addition, the combination of fluorescent agents with radiotracers could potential increase the accuracy of cancer staging and improve decision-making on antitumour treatments. These advances could drive a positive move towards reducing the high health-care costs related to oncology procedures, and improving the quality of cancer care.

Owing to the novelty of real-time fluorescent cancer detection strategies, many implementation barriers remain, including the feasibility of clinical applications, regulatory challenges, and considerations regarding clinical trial design. Thus, multidisciplinary collaboration between experts will be required to develop, translate, and realize the full clinical potential of fluorescent cancer detection.

Supplementary Material

Refer to Web version on PubMed Central for supplementary material.

Acknowledgments

References

1. Nguyen QT, Tsien RY. Fluorescence-guided surgery with live molecular navigation — a new cutting edge. Nat Rev Cancer. 2013; 13:653–662. [PubMed: 23924645]

2. Vahrmeijer AL, Hutteman M, van der Vorst JR, van de Velde CJ, Frangioni JV. Image-guided cancer surgery using near-infrared fluorescence. Nat Rev Clin Oncol. 2013; 10:507–518. [PubMed: 23881033]

3. Rosenthal EL, et al. Successful translation of fluorescence navigation during oncologic surgery: a consensus report. J Nucl Med. 2016; 57:144–150. [PubMed: 26449839]

4. Rosenthal EL, Warram JM, Bland KI, Zinn KR. The status of contemporary image-guided modalities in oncologic surgery. Ann Surg. 2015; 261:46–55. [PubMed: 25599326]

5. Yossepowitch O, et al. Positive surgical margins after radical prostatectomy: a systematic review and contemporary update. Eur Urol. 2014; 65:303–313. [PubMed: 23932439]

6. Swindle P, et al. Do margins matter? The prognostic significance of positive surgical margins in radical prostatectomy specimens. J Urol. 2005; 174:903–907. [PubMed: 16093984]

7. Winter JM, et al. 1423 pancreaticoduodenectomies for pancreatic cancer: a single-institution experience. J Gastrointest Surg. 2006; 10:1199–1211. [PubMed: 17114007]

8. McGirt MJ, et al. Extent of surgical resection is independently associated with survival in patients with hemispheric infiltrating low-grade gliomas. Neurosurgery. 2008; 63:700–708. [PubMed: 18981880]

9. Stummer W, et al. Fluorescence-guided surgery with 5-aminolevulinic acid for resection of malignant glioma: a randomised controlled multicentre phase III trial. Lancet Oncol. 2006; 7:392–401. [PubMed: 16648043]

10. Park CC, et al. Outcome at 8 years after breast-conserving surgery and radiation therapy for invasive breast cancer: influence of margin status and systemic therapy on local recurrence. J Clin Oncol. 2000; 18:1668–1675. [PubMed: 10764427]

11. McMahon J, et al. Influence of condition of surgical margins on local recurrence and disease-specific survival in oral and oropharyngeal cancer. Br J Oral Maxillofac Surg. 2003; 41:224–231. [PubMed: 12946663]

12. Ravasz LA, Slootweg PJ, Hordijk GJ, Smit F, van der Tweel I. The status of the resection margin as a prognostic factor in the treatment of head and neck carcinoma. J Craniomaxillofac Surg. 1991; 19:314–318. [PubMed: 1752972]

13. Lacroix M, et al. A multivariate analysis of 416 patients with glioblastoma multiforme: prognosis, extent of resection, and survival. J Neurosurg. 2001; 95:190–198.

14. McGirt MJ, et al. Independent association of extent of resection with survival in patients with malignant brain astrocytoma. J Neurosurg. 2009; 110:156–162. [PubMed: 18847342]

15. Frangioni JV. *In vivo* near-infrared fluorescence imaging. Curr Opin Chem Biol. 2003; 7:626–634. [PubMed: 14580568]

16. Cheong WF, Prahl SA, Welch AJ. A review of the optical properties of biological tissues. IEEE J Quantum Electron. 1990; 26:2166–2185.

17. Rosenthal EL, et al. Safety and tumor specificity of cetuximab-IRDye800 for surgical navigation in head and neck cancer. Clin Cancer Res. 2015; 21:3658–3666. [PubMed: 25904751]

18. Hope-Ross M, et al. Adverse reactions due to indocyanine green. Ophthalmology. 1994; 101:529–533. [PubMed: 8127574]

19. Marshall M, Draney D, Sevick-Muraca E, Olive DM. Single-dose intravenous toxicity study of IRDye 800CW in Sprague-Dawley rats. Mol Imaging Biol. 2010; 12:583–594. [PubMed: 20376568]

20. Obana A, et al. Survey of complications of indocyanine green angiography in Japan. Am J Ophthalmol. 1994; 118:749–753. [PubMed: 7977601]

21. Zhu B, Sevick-Muraca E. A review of performance of near-infrared fluorescence imaging devices used in clinical studies. Br J Radiol. 2014; 88:20140547.

22. Mondal SB, et al. Real-time fluorescence image-guided oncologic surgery. Adv Cancer Res. 2014; 124:171. [PubMed: 25287689]

23. Chi C, et al. Intraoperative imaging-guided cancer surgery: from current fluorescence molecular imaging methods to future multi-modality imaging technology. Theranostics. 2014; 4:1072–1084. [PubMed: 25250092]

24. O'Connor, JPB., et al. Imaging biomarker roadmap for cancer studies. Nat Rev Clin Oncol. 2016. http://dx.doi.org/10.1038/nrclinonc.2016.162

25. Tichauer KM, Wang Y, Pogue BW, Liu JT. Quantitative *in vivo* cell-surface receptor imaging in oncology: kinetic modeling and paired-agent principles from nuclear medicine and optical imaging. Phys Med Biol. 2015; 60:R239. [PubMed: 26134619]

26. Ilginis T, Clarke J, Patel PJ. Ophthalmic imaging. Br Med Bull. 2014; 111:77–88. [PubMed: 25139430]

27. Donald J, Gass M. Pathogenesis of disciform detachment of the neuroepithelium: IV. Fluorescein angiographic study of senile disciform macular degeneration. Am J Opthalmol. 1967; 63:645/73–659/87.

28. Polom K, et al. Current trends and emerging future of indocyanine green usage in surgery and oncology. Cancer. 2011; 117:4812–4822. [PubMed: 21484779]

29. Polom W, Markuszewski M, Rho YS, Matuszewski M. Usage of invisible near infrared light (NIR) fluorescence with indocyanine green (ICG) and methylene blue (MB) in urological oncology. Part 1. Cent European J Urol. 2014; 67:142–148.

30. Tummers QRJG, et al. Intraoperative near-infrared fluorescence imaging of a paraganglioma using methylene blue: a case report. Int J Surg Case Rep. 2015; 6:150–153.

31. Fidel J, et al. Preclinical validation of the utility of BLZ-100 in providing fluorescence contrast for imaging spontaneous solid tumors. Cancer Res. 2015; 75:4283–4291. [PubMed: 26471914]

32. Whitley MJ, et al. A mouse-human phase 1 co-clinical trial of a protease-activated fluorescent probe for imaging cancer. Sci Transl Med. 2016; 8:320ra4.

33. van Dam GM, et al. Intraoperative tumor-specific fluorescence imaging in ovarian cancer by folate receptor-α targeting: first in-human results. Nat Med. 2011; 17:1315–1319. [PubMed: 21926976]

34. De Jesus E, et al. Comparison of folate receptor targeted optical contrast agents for intraoperative molecular imaging. Int J Mol Imaging. 2015; 2015:469047. [PubMed: 26491562]

35. Garland M, Yim JJ, Bogyo MA. Bright future for precision medicine: advances in fluorescent chemical probe design and their clinical application. Cell Chem Biol. 2016; 23:122–136. [PubMed: 26933740]

36. Schaafsma BE, et al. The clinical use of indocyanine green as a near-infrared fluorescent contrast agent for image-guided oncologic surgery. J Surg Oncol. 2011; 104:323–332. [PubMed: 21495033]

37. Choi HS, et al. Targeted zwitterionic near-infrared fluorophores for improved optical imaging. Nat Biotechnol. 2013; 31:148–153. [PubMed: 23292608]

38. Mordon S, Devoisselle JM, Soulie-Begu S, Desmettre T. Indocyanine green: physicochemical factors affecting its fluorescencein vivo. Microvasc Res. 1998; 55:146–152. [PubMed: 9521889]

39. Desmettre T, Devoisselle JM, Mordon S. Fluorescence properties and metabolic features of indocyanine green (ICG) as related to angiography. Surv Ophthalmol. 2000; 45:15–27. [PubMed: 10946079]

40. Cousins A, Thompson SK, Wedding AB, Thierry B. Clinical relevance of novel imaging technologies for sentinel lymph node identification and staging. Biotechnol Adv. 2014; 32:269–279. [PubMed: 24189095]

41. Murawa D, Hirche C, Dresel S, Hünerbein M. Sentinel lymph node biopsy in breast cancer guided by indocyanine green fluorescence. Br J Surg. 2009; 96:1289–1294. [PubMed: 19847873]

42. Tagaya N, et al. Intraoperative identification of sentinel lymph nodes by near-infrared fluorescence imaging in patients with breast cancer. Am J Surg. 2008; 195:850–853. [PubMed: 18353274]

43. Sugie T, et al. Comparison of the indocyanine green fluorescence and blue dye methods in detection of sentinel lymph nodes in early-stage breast cancer. Ann Surg Oncol. 2013; 20:2213–2218. [PubMed: 23429938]

44. Sinno AK, Fader AN, Roche KL, Giuntoli RL II, Tanner EJ. A comparison of colorimetric versus fluorometric sentinel lymph node mapping during robotic surgery for endometrial cancer. Gynecol Oncol. 2014; 134:281–286. [PubMed: 24882555]

45. Schaafsma BE, et al. Randomized comparison of near-infrared fluorescence lymphatic tracers for sentinel lymph node mapping of cervical cancer. Gynecol Oncol. 2012; 127:126–130. [PubMed: 22796548]

46. Jung SY, et al. Comparison of sentinel lymph node biopsy guided by the multimodal method of indocyanine green fluorescence, radioisotope, and blue dye versus the radioisotope method in breast cancer: a randomized controlled trial. Ann Surg Oncol. 2013; 21:1254–1259. [PubMed: 24356798]

47. How J, et al. Comparing indocyanine green, technetium and blue dye for sentinel lymph node mapping in endometrial cancer. Gynecol Oncol. 2015; 137:436–442. [PubMed: 25870917]

48. Brouwer OR, et al. A hybrid radioactive and fluorescent tracer for sentinel node biopsy in penile carcinoma as a potential replacement for blue dye. Eur Urol. 2014; 65:600–609. [PubMed: 24355132]

49. Peloso A, et al. Combined use of intraoperative ultrasound and indocyanine green fluorescence imaging to detect liver metastases from colorectal cancer. HPB. 2013; 15:928–934. [PubMed: 23458105]

50. Gotoh K, et al. A novel image-guided surgery of hepatocellular carcinoma by indocyanine green fluorescence imaging navigation. J Surg Oncol. 2009; 100:75–79. [PubMed: 19301311]

51. Morita Y, et al. Detection of hepatocellular carcinomas with near-infrared fluorescence imaging using indocyanine green: its usefulness and limitation. Int J Clin Oncol. 2013; 18:232–241. [PubMed: 22200990]

52. Osayi SN, et al. Near-infrared fluorescent cholangiography facilitates identification of biliary anatomy during laparoscopic cholecystectomy. Surg Endosc. 2014; 29:368–375. [PubMed: 24986018]

53. Tummers QRJG, et al. The value of intraoperative near-infrared fluorescence imaging based on enhanced permeability and retention of indocyanine green: feasibility and false-positives in ovarian cancer. PLoS ONE. 2015; 10:e0129766. [PubMed: 26110901]

54. Hutteman M, et al. Near-infrared fluorescence imaging in patients undergoing pancreaticoduodenectomy. Eur Surg Res. 2011; 47:90–97. [PubMed: 21720166]

55. Liberale G, et al. Fluorescence imaging after indocyanine green injection for detection of peritoneal metastases in patients undergoing cytoreductive surgery for peritoneal carcinomatosis from colorectal cancer: a pilot study. Ann Surg. 2016; 264:1110–1115. [PubMed: 27828822]

56. Shepherd M, Dailey HA. A continuous fluorimetric assay for protoporphyrinogen oxidase by monitoring porphyrin accumulation. Anal Biochem. 2005; 344:115–121. [PubMed: 16039600]

57. Dolmans DE, Fukumura D, Jain RK. Photodynamic therapy for cancer. Nat Rev Cancer. 2003; 3:380–387. [PubMed: 12724736]

58. Soler AM, Warloe T, Berner A, Giercksky KE. A follow-up study of recurrence and cosmesis in completely responding superficial and nodular basal cell carcinomas treated with methyl 5-aminolaevulinate-based photodynamic therapy alone and with prior curettage. Br J Dermatol. 2001; 145:467–471. [PubMed: 11531838]

59. Morton CA, et al. Comparison of photodynamic therapy with cryotherapy in the treatment of Bowen's disease. Br J Dermatol. 1996; 135:766–771. [PubMed: 8977678]

60. Szeimies RM, Sassy T, Landthaler M. Penetration potency of topical applied δ-aminolevulinic acid for photodynamic therapy of basal cell carcinoma. Photochem Photobiol. 1994; 59:73–76. [PubMed: 8127943]

61. Dögnitz N, et al. Comparison of ALA-and ALA hexyl-ester-induced PpIX depth distribution in human skin carcinoma. J Photochem Photobiol B. 2008; 93:140–148. [PubMed: 18818091]

62. Perrett CM, et al. Treatment of post-transplant premalignant skin disease: a randomized intrapatient comparative study of 5-fluorouracil cream and topical photodynamic therapy. Br J Dermatol. 2007; 156:320–328. [PubMed: 17223873]

63. Regula J, et al. Photosensitisation and photodynamic therapy of oesophageal, duodenal, and colorectal tumours using 5 aminolaevulinic acid induced protoporphyrin IX — a pilot study. Gut. 1995; 36:67–75. [PubMed: 7890239]

64. Vinciullo C, et al. Photodynamic therapy with topical methyl aminolaevulinate for 'difficult-to-treat' basal cell carcinoma. Br J Dermatol. 2005; 152:765–772. [PubMed: 15840111]

65. Gossner L, et al. Photodynamic ablation of high-grade dysplasia and early cancer in Barrett's esophagus by means of 5-aminolevulinic acid. Gastroenterology. 1998; 114:448–455. [PubMed: 9496934]

66. Juarranz Á, Jaén P, Sanz-Rodríguez F, Cuevas J, González S. Photodynamic therapy of cancer. Basic principles and applications. Clin Transl Oncol. 2008; 10:148–154. [PubMed: 18321817]

67. Peng Q, et al. Distribution of 5-aminolevulinic acid-induced porphyrins in noduloulcerative basal cell carcinoma. Photochem Photobiol. 1995; 62:906–913. [PubMed: 8570730]

68. Juzeniene A, Juzenas P, Ma LW, Iani V, Moan J. Topical application of 5-aminolaevulinic acid, methyl 5-aminolaevulinate and hexyl 5-aminolaevulinate on normal human skin. Br J Dermatol. 2006; 155:791–799. [PubMed: 16965430]

69. Matsui A, et al. Real-time, near-infrared, fluorescence-guided identification of the ureters using methylene blue. Surgery. 2010; 148:78–86. [PubMed: 20117811]

70. Cenens J, Schoonheydt R. Visible spectroscopy of methylene blue on hectorite, laponite B, and barasym in aqueous suspension. Clays Clay Miner. 1988; 36:214–224.

71. Mohr H, Knüver-Hopf J, Gravemann U, Redecker-Klein A, Müller TH. West Nile virus in plasma is highly sensitive to methylene blue–light treatment. Transfusion. 2004; 44:886–890. [PubMed: 15157256]

72. Vorst JR, et al. Intraoperative near-infrared fluorescence imaging of parathyroid adenomas with use of low-dose methylene blue. Head Neck. 2014; 36:853–858. [PubMed: 23720199]

73. Traynor S, Adams JR, Andersen P, Everts E, Cohen J. Appropriate timing and velocity of infusion for the selective staining of parathyroid glands by intravenous methylene blue. Am J Surg. 1998; 176:15–17. [PubMed: 9683125]

74. Winer JH, et al. Intraoperative localization of insulinoma and normal pancreas using invisible near-infrared fluorescent light. Ann Surg Oncol. 2010; 17:1094–1100. [PubMed: 20033320]

75. van der Vorst JR, et al. Near-infrared fluorescence imaging of a solitary fibrous tumor of the pancreas using methylene blue. World J Gastrointest Surg. 2012; 4:180. [PubMed: 22905287]

76. Tardivo JP, et al. Methylene blue in photodynamic therapy: from basic mechanisms to clinical applications. Photodiagnosis Photodyn Ther. 2005; 2:175–191. [PubMed: 25048768]

77. Müller-Breitkreutz K, Mohr H. Hepatitis C and human immunodeficiency virus RNA degradation by methylene blue/light treatment of human plasma. J Med Virol. 1998; 56:239–245. [PubMed: 9783692]

78. Zolfaghari PS, et al. In vivo killing of *Staphylococcus aureus* using a light-activated antimicrobial agent. BMC Microbiol. 2009; 9:27–27. [PubMed: 19193212]

79. Kobayashi H, Ogawa M, Alford R, Choyke PL, Urano Y. New strategies for fluorescent probe design in medical diagnostic imaging. Chem Rev. 2009; 110:2620–2640.

80. Chance B. Near-infrared images using continuous, phase-modulated, and pulsed light with quantitation of blood and blood oxygenation. Ann NY Acad Sci. 1998; 838:29–45. [PubMed: 9511793]

81. Ptaszek M. Rational design of fluorophores for *in vivo* applications. Prog Mol Biol Transl Sci. 2013; 113:59–108. [PubMed: 23244789]

82. Ogawa M, Kosaka N, Choyke PL, Kobayashi H. *In vivo* molecular imaging of cancer with a quenching near-infrared fluorescent probe using conjugates of monoclonal antibodies and indocyanine green. Cancer Res. 2009; 69:1268–1272. [PubMed: 19176373]

83. Yi X, Wang F, Qin W, Yang X, Yuan J. Near-infrared fluorescent probes in cancer imaging and therapy: an emerging field. Int J Nanomedicine. 2014; 9:1347–1365. [PubMed: 24648733]

84. Soper SA, Mattingly QL. Steady-state and picosecond laser fluorescence studies of nonradiative pathways in tricarbocyanine dyes: implications to the design of near-IR fluorochromes with high fluorescence efficiencies. J Am Chem Soc. 1994; 116:3744–3752.

85. Altınoğˇlu EI, et al. Near-infrared emitting fluorophore-doped calcium phosphate nanoparticles for *in vivo* imaging of human breast cancer. ACS Nano. 2008; 2:2075–2084. [PubMed: 19206454]

86. Levitus M, Ranjit S. Cyanine dyes in biophysical research: the photophysics of polymethine fluorescent dyes in biomolecular environments. Q Rev Biophys. 2011; 44:123–151. [PubMed: 21108866]

87. Strekowski L, Lipowska M, Patonay G. Substitution reactions of a nucleofugal group in heptamethine cyanine dyes. Synthesis of an isothiocyanato derivative for labeling of proteins with a near-infrared chromophore. J Org Chem. 1992; 57:4578–4580.

88. Tyutyulkov, N. Polymethine Dyes: Structure and Properties. St. Kliment Ohridski Univ. Press; 1991.

89. Mujumdar RB, Ernst LA, Mujumdar SR, Lewis CJ, Waggoner AS. Cyanine dye labeling reagents: sulfoindocyanine succinimidyl esters. Bioconjug Chem. 1993; 4:105–111. [PubMed: 7873641]

90. Choi HS, et al. Synthesis and *in vivo* fate of zwitterionic near-infrared fluorophores. Angew Chem Int Ed. 2011; 50:6258–6263.

91. Umezawa K, Citterio D, Suzuki K. New trends in near-infrared fluorophores for bioimaging. Anal Sci. 2014; 30:327–349. [PubMed: 24614728]

92. Antaris AL, et al. A small-molecule dye for NIR-II imaging. Nat Mater. 2016; 15:235–242. [PubMed: 26595119]

93. Qi S, et al. Evaluation of four affibody-based near-infrared fluorescent probes for optical imaging of epidermal growth factor receptor positive tumors. Bioconjug Chem. 2012; 23:1149–1156. [PubMed: 22621238]

94. Sano K, et al. Short PEG-linkers improve the performance of targeted, activatable monoclonal antibody-indocyanine green optical imaging probes. Bioconjug Chem. 2013; 24:811–816. [PubMed: 23600922]

95. Kobayashi H, Choyke PL. Target-cancer-cell-specific activatable fluorescence imaging probes: rational design and *in vivo* applications. Acc Chem Res. 2010; 44:83–90. [PubMed: 21062101]

96. Winnard P, Raman V. Real time non-invasive imaging of receptor–ligand interactions *in vivo*. J Cell Biochem. 2003; 90:454–463. [PubMed: 14523979]

97. Barrett T, et al. In vivo diagnosis of epidermal growth factor receptor expression using molecular imaging with a cocktail of optically labeled monoclonal antibodies. Clin Cancer Res. 2007; 13:6639–6648. [PubMed: 17982120]

98. Wu AM, Senter PD. Arming antibodies: prospects and challenges for immunoconjugates. Nat Biotechnol. 2005; 23:1137–1146. [PubMed: 16151407]

99. Srinivasarao M, Galliford CV, Low PS. Principles in the design of ligand-targeted cancer therapeutics and imaging agents. Nat Rev Drug Discov. 2015; 14:203–219. [PubMed: 25698644]

100. Talvensaari-Mattila A, Pääkkö P, Turpeenniemi-Hujanen T. Matrix metalloproteinase-2 (MMP-2) is associated with survival in breast carcinoma. Br J Cancer. 2003; 89:1270–1275. [PubMed: 14520459]

101. Mohamed MM, Sloane BF. Cysteine cathepsins: multifunctional enzymes in cancer. Nat Rev Cancer. 2006; 6:764–775. [PubMed: 16990854]

102. Parks WC, Wilson CL, López-Boado YS. Matrix metalloproteinases as modulators of inflammation and innate immunity. Nat Rev Immunol. 2004; 4:617–629. [PubMed: 15286728]

103. Coussens LM, Werb Z. Inflammation and cancer. Nature. 2002; 420:860–867. [PubMed: 12490959]

104. Urano Y, et al. Rapid cancer detection by topically spraying a γ-glutamyltranspeptidase–activated fluorescent probe. Sci Transl Med. 2011; 3:110ra119.

105. Jiang T, et al. Tumor imaging by means of proteolytic activation of cell-penetrating peptides. Proc Natl Acad Sci USA. 2004; 101:17867–17872. [PubMed: 15601762]

106. Savariar EN, et al. Real-time *in vivo* molecular detection of primary tumors and metastases with ratiometric activatable cell-penetrating peptides. Cancer Res. 2013; 73:855–864. [PubMed: 23188503]

107. Gu FX, et al. Targeted nanoparticles for cancer therapy. Nano Today. 2007; 2:14–21.

108. Muyldermans S. Nanobodies: natural single-domain antibodies. Annu Rev Biochem. 2013; 82:775–797. [PubMed: 23495938]

109. Devaraj NK, Upadhyay R, Haun JB, Hilderbrand SA, Weissleder R. Fast and sensitive pretargeted labeling of cancer cells through a tetrazine/trans-cyclooctene cycloaddition. Angew Chem Int Ed. 2009; 48:7013–7016.

110. Devaraj NK, Weissleder R. Biomedical applications of tetrazine cycloadditions. Acc Chem Res. 2011; 44:816–827. [PubMed: 21627112]

111. Reagan-Shaw S, Nihal M, Ahmad N. Dose translation from animal to human studies revisited. FASEB J. 2008; 22:659–661. [PubMed: 17942826]

112. Le Tourneau C, Lee JJ, Siu LL. Dose escalation methods in phase I cancer clinical trials. J Natl Cancer Inst. 2009; 101:708–720. [PubMed: 19436029]

113. Vacchelli E, et al. Trial Watch: tumor-targeting monoclonal antibodies in cancer therapy. Oncoimmunology. 2014; 3:e27048. [PubMed: 24605265]

114. Tjalma JJ, et al. Molecular fluorescence guided endoscopy targeting vascular endothelial growth factor A for improved colorectal polyp detection. J Nucl Med. 2016; 57:480–485. [PubMed: 26678613]

115. Day KE, Sweeny L, Kulbersh B, Zinn KR, Rosenthal EL. Preclinical comparison of near-infrared-labeled cetuximab and panitumumab for optical imaging of head and neck squamous cell carcinoma. Mol Imaging Biol. 2013; 15:722–729. [PubMed: 23715932]

116. Grandis JR, Tweardy DJ. Elevated levels of transforming growth factor α and epidermal growth factor receptor messenger RNA are early markers of carcinogenesis in head and neck cancer. Cancer Res. 1993; 53:3579–3584. [PubMed: 8339264]

117. Wright GL, Haley C, Beckett ML, Schellhammer PF. Expression of prostate-specific membrane antigen in normal, benign, and malignant prostate tissues. Urol Oncol. 1995; 1:18–28. [PubMed: 21224086]

118. Israeli RS, Powell CT, Corr JG, Fair WR, Heston WD. Expression of the prostate-specific membrane antigen. Cancer Res. 1994; 54:1807–1811. [PubMed: 7511053]

119. Bander NH, et al. Targeting metastatic prostate cancer with radiolabeled monoclonal antibody J591 to the extracellular domain of prostate specific membrane antigen. J Urol. 2003; 170:1717–1721. [PubMed: 14532761]

120. Van den Ouden D, Bentvelsen FM, Boeve ER, Schroder FH. Positive margins after radical prostatectomy: correlation with local recurrence and distant progression. Br J Urol. 1993; 72:489–494. [PubMed: 7505193]

121. Nakajima T, et al. Targeted, activatable. *in vivo* fluorescence imaging of prostate-specific membrane antigen (PSMA) positive tumors using the quenched humanized J591 antibody–indocyanine green (ICG) conjugate. Bioconjug Chem. 2011; 22:1700–1705. [PubMed: 21740058]

122. Butte PV, et al. Near-infrared imaging of brain tumors using the Tumor Paint BLZ-100 to achieve near-complete resection of brain tumors. Neurosurg Focus. 2014; 36:E1.

123. Baik FM, et al. Fluorescence identification of head and neck squamous cell carcinoma and high-risk oral dysplasia with BLZ-100, a chlorotoxin-indocyanine green conjugate. JAMA Otolaryngol Head Neck Surg. 2016; 142:330–338. [PubMed: 26892902]

124. Verbeek FP, et al. Sentinel lymph node biopsy in vulvar cancer using combined radioactive and fluorescence guidance. Int J Gynecol Cancer. 2015; 25:1086–1093. [PubMed: 25768079]

125. Burggraaf J, et al. Detection of colorectal polyps in humans using an intravenously administered fluorescent peptide targeted against c-Met. Nat Med. 2015; 21:955–961. [PubMed: 26168295]

126. Dutch Central Committee on Research Involving Human Subjects. 2012. No authors listed. ABR-formulier NL32320.058.10https://www.toetsingonline.nl/to/ccmo_search.nsf/fABRpop?readform&unids=C1257BA2002CC066C1257884003FEF1F

127. Parker N, et al. Folate receptor expression in carcinomas and normal tissues determined by a quantitative radioligand binding assay. Anal Biochem. 2005; 338:284–293. [PubMed: 15745749]

128. Tummers Q, et al. Intraoperative imaging of folate receptor alpha positive ovarian and breast cancer using the tumor specific agent EC17. Oncotarget. 2016; 7:32144–32155. [PubMed: 27014973]

129. Boogerd L, et al. Concordance of folate receptor-α expression between biopsy, primary tumor and metastasis in breast cancer and lung cancer patients. Oncotarget. 2016; 7:17442–17454. [PubMed: 26943581]

130. Weichert JP, et al. Alkylphosphocholine analogs for broad-spectrum cancer imaging and therapy. Sci Transl Med. 2014; 6:240ra75.

131. Deming DA, et al. Phospholipid ether analogs for the detection of colorectal tumors. PLoS ONE. 2014; 9:e109668. [PubMed: 25286226]

132. Korb ML, et al. Breast cancer imaging using the near-infrared fluorescent agent, CLR1502. Mol Imaging. 2014; 13

133. Swanson KI, et al. Fluorescent cancer-selective alkylphosphocholine analogs for intraoperative glioma detection. Neurosurgery. 2015; 76:115–124. [PubMed: 25549194]

134. Zhang RR, Swanson KI, Hall LT, Weichert JP, Kuo JS. Diapeutic cancer-targeting alkylphosphocholine analogs may advance management of brain malignancies. CNS Oncol. 2016; 5:223–231. [PubMed: 27616199]

135. Grudzinski JJ, et al. A phase 1 study of 131I-CLR1404 in patients with relapsed or refractory advanced solid tumors: dosimetry, biodistribution, pharmacokinetics, and safety. PLoS ONE. 2014; 9:e111652. [PubMed: 25402488]

136. Lubner SJ, et al. A phase 1, multi-center, open-label, dose-escalation study of I-CLR1404 in subjects with relapsed or refractory advanced solid malignancies. Cancer Invest. 2015; 33:483–489. [PubMed: 26536061]

137. Lee, WD., Bawendi, MG., Ferrer, J. Imaging agent for detection of diseased cells. US Patent 20,140,301,950. 2014. p. A1

138. Hussain T, et al. Surgical molecular navigation with a ratiometric activatable cell penetrating peptide improves intraoperative identification and resection of small salivary gland cancers. Head Neck. 2016; 38:715–723. [PubMed: 25521629]

139. Metildi CA, et al. Ratiometric activatable cell-penetrating peptides label pancreatic cancer, enabling fluorescence-guided surgery, which reduces metastases and recurrence in orthotopic mouse models. Ann Surg Oncol. 2015; 22:2082–2087. [PubMed: 25319581]

140. Urano Y, et al. Selective molecular imaging of viable cancer cells with pH-activatable fluorescence probes. Nat Med. 2009; 15:104–109. [PubMed: 19029979]

141. Lee H, et al. Near-infrared pH-activatable fluorescent probes for imaging primary and metastatic breast tumors. Bioconjug Chem. 2011; 22:777–784. [PubMed: 21388195]

142. Tan X, et al. A NIR heptamethine dye with intrinsic cancer targeting, imaging and photosensitizing properties. Biomaterials. 2012; 33:2230–2239. [PubMed: 22182749]

143. Yang X, et al. Near IR heptamethine cyanine dye– mediated cancer imaging. Clin Cancer Res. 2010; 16:2833–2844. [PubMed: 20410058]

144. Yang X, et al. Optical imaging of kidney cancer with novel near infrared heptamethine carbocyanine fluorescent dyes. J Urol. 2013; 189:702–710. [PubMed: 23000848]

145. Henary M, Pannu V, Owens EA, Aneja R. Near infrared active heptacyanine dyes with unique cancer-imaging and cytotoxic properties. Bioorg Med Chem Lett. 2012; 22:1242–1246. [PubMed: 22177785]

146. Trivedi ER, et al. Chiral porphyrazine near-IR optical imaging agent exhibiting preferential tumor accumulation. Proc Natl Acad Sci USA. 2010; 107:1284–1288. [PubMed: 20080563]

147. Zhang C, et al. A near-infrared fluorescent heptamethine indocyanine dye with preferential tumor accumulation for *in vivo* imaging. Biomaterials. 2010; 31:6612–6617. [PubMed: 20542559]

148. Wu JB, et al. Near-infrared fluorescence imaging of cancer mediated by tumor hypoxia and HIF1α/OATPs signaling axis. Biomaterials. 2014; 35:8175–8185. [PubMed: 24957295]

149. Shimada S, Ohtsubo S, Ogasawara K, Kusano M. Macro- and microscopic findings of ICG fluorescence in liver tumors. World J Surg Oncol. 2015; 13:198. [PubMed: 26055754]

150. Tummers QRJG, et al. Intraoperative guidance in parathyroid surgery using near-infrared fluorescence imaging and low-dose methylene blue. Surgery. 2015; 158:1323–1330. [PubMed: 25958068]

151. Gibbs-Strauss SL, et al. Nerve-highlighting fluorescent contrast agents for image-guided surgery. Mol Imaging. 2011; 10:91–101. [PubMed: 21439254]

152. Park MH, et al. Prototype nerve-specific near-infrared fluorophores. Theranostics. 2014; 4:823–833. [PubMed: 24955143]

153. Hyun H, et al. Structure-inherent targeting of near-infrared fluorophores for parathyroid and thyroid gland imaging. Nat Med. 2015; 21:192–197. [PubMed: 25559343]

154. Tichauer KM, et al. Microscopic lymph node tumor burden quantified by macroscopic dual-tracer molecular imaging. Nat Med. 2014; 20:1348–1353. [PubMed: 25344739]

155. van den Berg NS, et al. Multimodal surgical guidance during sentinel node biopsy for melanoma: combined gamma tracing and fluorescence imaging of the sentinel node through use of the hybrid tracer indocyanine green – 99mTc-nanocolloid. Radiology. 2014; 275:521–529. [PubMed: 25521776]

156. Hekman MCH, et al. Targeted dual-modality imaging in renal cell carcinoma: an *ex vivo* kidney perfusion study. Clin Cancer Res. 2016; 15:4634–4642.

157. Bui MH, et al. Carbonic anhydrase IX is an independent predictor of survival in advanced renal clear cell carcinoma implications for prognosis and therapy. Clin Cancer Res. 2003; 9:802–811. [PubMed: 12576453]

158. Nayak TK, Garmestani K, Baidoo KE, Milenic DE, Brechbiel MW. PET imaging of tumor angiogenesis in mice with VEGF-A–targeted [86]Y-CHX-A″-DTPA-bevacizumab. Int J Cancer. 2011; 128:920–926. [PubMed: 20473899]

159. Nayak TK, et al. PET imaging of HER1-expressing xenografts in mice with 86Y-CHX-A″-DTPA-cetuximab. Eur J Nucl Med Mol Imaging. 2010; 37:1368–1376. [PubMed: 20155263]

160. Mieog JSD, et al. Toward optimization of imaging system and lymphatic tracer for near-infrared fluorescent sentinel lymph node mapping in breast cancer. Ann Surg Oncol. 2011; 18:2483–2491. [PubMed: 21360250]

161. Troyan SL, et al. The FLARE™ intraoperative near-infrared fluorescence imaging system: a first-in-human clinical trial in breast cancer sentinel lymph node mapping. Ann Surg Oncol. 2009; 16:2943–2952. [PubMed: 19582506]

162. Themelis G, Yoo JS, Soh KS, Schulz R, Ntziachristos V. Real-time intraoperative fluorescence imaging system using light-absorption correction. J Biomed Opt. 2009; 14:064012. [PubMed: 20059250]

163. Schols RM, Connell NJ, Stassen LP. Near-infrared fluorescence imaging for real-time intraoperative anatomical guidance in minimally invasive surgery: a systematic review of the literature. World J Surg. 2015; 39:1069–1079. [PubMed: 25522896]

164. Aoki T, et al. Intraoperative fluorescent imaging using indocyanine green for liver mapping and cholangiography. J Hepatobiliary Pancreat Sci. 2010; 17:590–594. [PubMed: 19844652]

165. Schols RM, et al. Combined vascular and biliary fluorescence imaging in laparoscopic cholecystectomy. Surg Endosc. 2013; 27:4511–4517. [PubMed: 23877766]

166. Tonn JC, Stummer W. Fluorescence-guided resection of malignant gliomas using 5-aminolevulinic acid: practical use, risks, and pitfalls. Clin Neurosurg. 2008; 55:20–26. [PubMed: 19248665]

167. Kitai T, Kawashima M. Transcutaneous detection and direct approach to the sentinel node using axillary compression technique in ICG fluorescence-navigated sentinel node biopsy for breast cancer. Breast Cancer. 2011; 19:343–348. [PubMed: 21725656]

168. Zhu N, et al. Engineering light-emitting diode surgical light for near-infrared fluorescence image-guided surgical systems. J Biomed Opt. 2014; 19:076018. [PubMed: 25057962]

169. Keereweer S, et al. Image-guided surgery in head and neck cancer: current practice and future directions of optical imaging. Head Neck. 2012; 34:120–126. [PubMed: 21284051]

170. D'Souza AV, Lin H, Henderson ER, Samkoe KS, Pogue BW. Review of fluorescence guided surgery systems: identification of key performance capabilities beyond indocyanine green imaging. J Biomed Opt. 2016; 21:080901.

171. Mito JK, et al. Intraoperative detection and removal of microscopic residual sarcoma using wide-field imaging. Cancer. 2012; 118:5320–5330. [PubMed: 22437667]

172. Food, US., Administration, Drug. Guidance for industry, investigators, and reviewers. Exploratory IND studies. FDA. 2006. http://www.fda.gov/downloads/Drugs/GuidanceComplianceRegulatoryInformation/Guidances/UCM078933.pdf

173. Moan J, Streckyte G, Bagdonas S, Bech Ø, Berg K. Photobleaching of protoporphyrin IX in cells incubated with 5-aminolevulinic acid. Int J Cancer. 1997; 70:90–97. [PubMed: 8985096]

174. Dragieva G, et al. Topical photodynamic therapy in the treatment of actinic keratoses and Bowen's disease in transplant recipients. Transplantation. 2004; 77:115–121. [PubMed: 14724445]

175. Angell-Petersen E, et al. Porphyrin formation in actinic keratosis and basal cell carcinoma after topical application of methyl 5-aminolevulinate. J Invest Dermatol. 2006; 126:265–271. [PubMed: 16374471]

176. Rhodes LE, et al. Photodynamic therapy using topical methyl aminolevulinate versus surgeryfor nodular basal cell carcinoma: results of a multicenter randomized prospective trial. Arch Dermatol. 2004; 140:17–23. [PubMed: 14732655]

177. Ceilley RI, Del Rosso JQ. Current modalities and new advances in the treatment of basal cell carcinoma. Int J Dermatol. 2006; 45:489–498. [PubMed: 16700779]

178. Willey A, Mehta S, Lee PK. Reduction in the incidence of squamous cell carcinoma in solid organ transplant recipients treated with cyclic photodynamic therapy. Dermatol Surg. 2010; 36:652–658. [PubMed: 19889154]

179. Leunig A, et al. Detection of squamous cell carcinoma of the oral cavity by imaging 5-aminolevulinic acid-induced protoporphyrin ix fluorescence. Laryngoscope. 2000; 110:78–83. [PubMed: 10646720]

180. Frank R, Bos J. Photodynamic therapy for condylomata acuminata with local application of 5-aminolevulinic acid. Genitourin Med. 1996; 72:70–71. [PubMed: 8655176]

181. Mayerhöffer U, Fimmel B, Würthner F. Bright near-infrared fluorophores based on squaraines by unexpected halogen effects. Angew Chem Int Ed. 2012; 51:164–167.

182. Arunkumar E, Forbes CC, Noll BC, Smith BD. Squaraine-derived rotaxanes: sterically protected fluorescent near-IR dyes. J Am Chem Soc. 2005; 127:3288–3289. [PubMed: 15755140]

183. Zhang X, Yu H, Xiao Y. Replacing phenyl ring with thiophene: an approach to longer wavelength aza-dipyrromethene boron difluoride (aza-BODIPY) dyes. J Org Chem. 2011; 77:669–673. [PubMed: 22111977]

184. Umezawa K, Matsui A, Nakamura Y, Citterio D, Suzuki K. Bright, color-tunable fluorescent dyes in the Vis/NIR region: establishment of new "tailor-made" multicolor fluorophores based on borondipyrromethene. Chemistry. 2009; 15:1096–1106. [PubMed: 19117043]

185. Koide Y, et al. Development of NIR fluorescent dyes based on Si–rhodamine for *in vivo* imaging. J Am Chem Soc. 2012; 134:5029–5031. [PubMed: 22390359]

186. Arden-Jacob J, Drexhage K, Frantzeskos J, Zilles A. Neue Carbopyronin-Fluoreszenz-Farbstoffe, PCT patent application WO 00/64986. Chem Abstr. 2000:336553.

187. Yang E, et al. Photophysical properties and electronic structure of stable, tunable synthetic bacteriochlorins: extending the features of native photosynthetic pigments. J Phys Chem B. 2011; 115:10801–10816. [PubMed: 21875047]

188. Kobayashi, M., Akiyama, M., Kano, H., Kise, H. Chlorophylls and Bacteriochlorophylls. Grimm, B.Porra, RJ.Rudiger, W., Scheer, H., editors. Springer; 2006. p. 79-94.

189. Liu Y, et al. Intraoperative detection of liver tumors aided by a fluorescence goggle system and multimodal imaging. Analyst. 2013; 138:2254–2257. [PubMed: 23467534]

190. Kubota K, et al. Intraoperative assessment of reconstructed vessels in living-donor liver transplantation, using a novel fluorescence imaging technique. J Hepatobiliary Pancreat Surg. 2006; 13:100–104. [PubMed: 16547669]

191. Kubota K, et al. Application of the HyperEye Medical System for esophageal cancer surgery: a preliminary report. Surg Today. 2013; 43:215–220. [PubMed: 22782594]

192. Tobergte, A., et al. The sigma.7 haptic interface for MiroSurge: a new bi-manual surgical console. IEEE/RSJ International Conference on Intelligent Robots and Systems. 2011. http://dx.doi.org/10.1109/IROS.2011.6094433

Key points

- Fluorescence imaging can transform the way surgeries are performed, through the intraoperative identification of vital structures, lymph nodes and cancer in real time

- Near-infrared (NIR) fluorescence is particularly advantageous for use in clinical settings owing to improved depth penetration and low autofluorescence in the NIR wavelength range compared with shorter wavelengths

- Many targeted NIR fluorophores are currently in preclinical development; however, no cancer-targeted NIR fluorophores or devices for intraoperative NIR fluorescence detection of cancer have received commercial approval for human use

- Multiple early phase clinical trials are underway to evaluate targeted fluorophores for real-time, intraoperative cancer detection in humans

- The use of targeted fluorophores for the intraoperative detection of cancer might improve survival rates and functional outcomes in patients with cancer

- Currently, substantial regulatory challenges and clinical trial considerations constitute barriers for the adoption of fluorescence-guided surgery in clinical settings
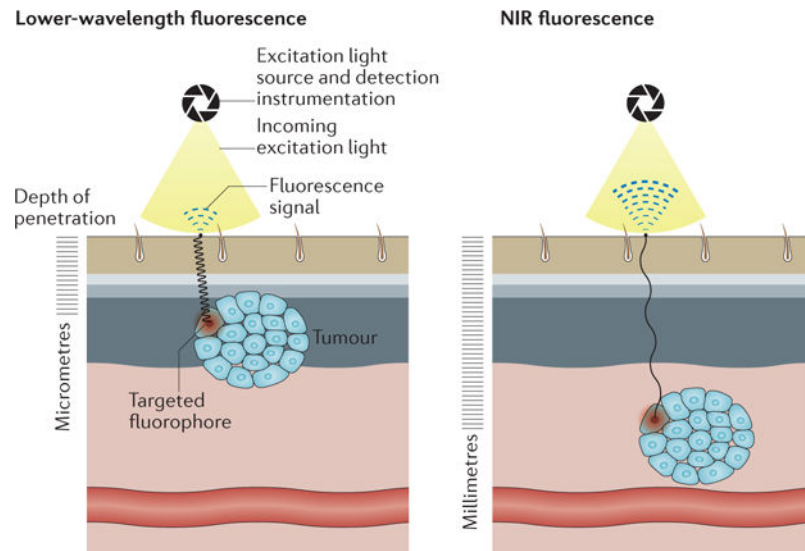
Figure 1. NIR fluorescence is more suitable for *in vivo* imaging applications than visible-light fluorescence

Near-infrared (NIR) fluorophores (700–900 nm) have deeper tissue penetration and lower background fluorescence than visible-light fluorescence, resulting in enhanced signal-to-noise ratios. The detection depths achievable with the currently available instrumentation ranges from millimeters with NIR fluorescence to micrometers with visible-range fluorescence.
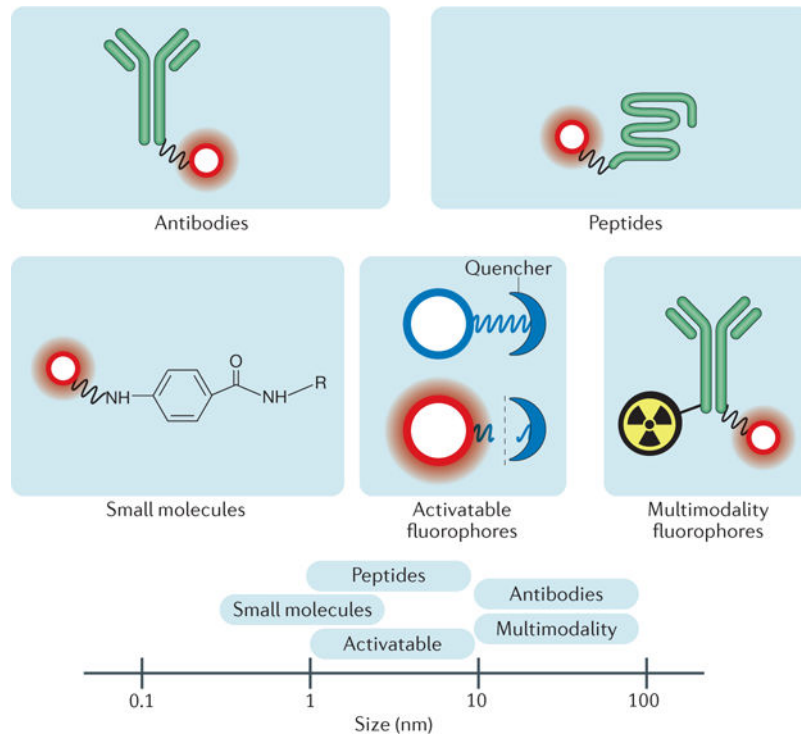
Figure 2. Targeted fluorophores tested in clinical trials
Targeted fluorophores currently tested in clinical trials include small molecules, peptides, activatable fluorophores, antibodies, and multimodal fluorophores. Activatable fluorophores are initially quenched, but upon cleavage by enzymes, emit fluorescence. The relative sizes of these targeted fluorophores are displayed in the bottom panel.
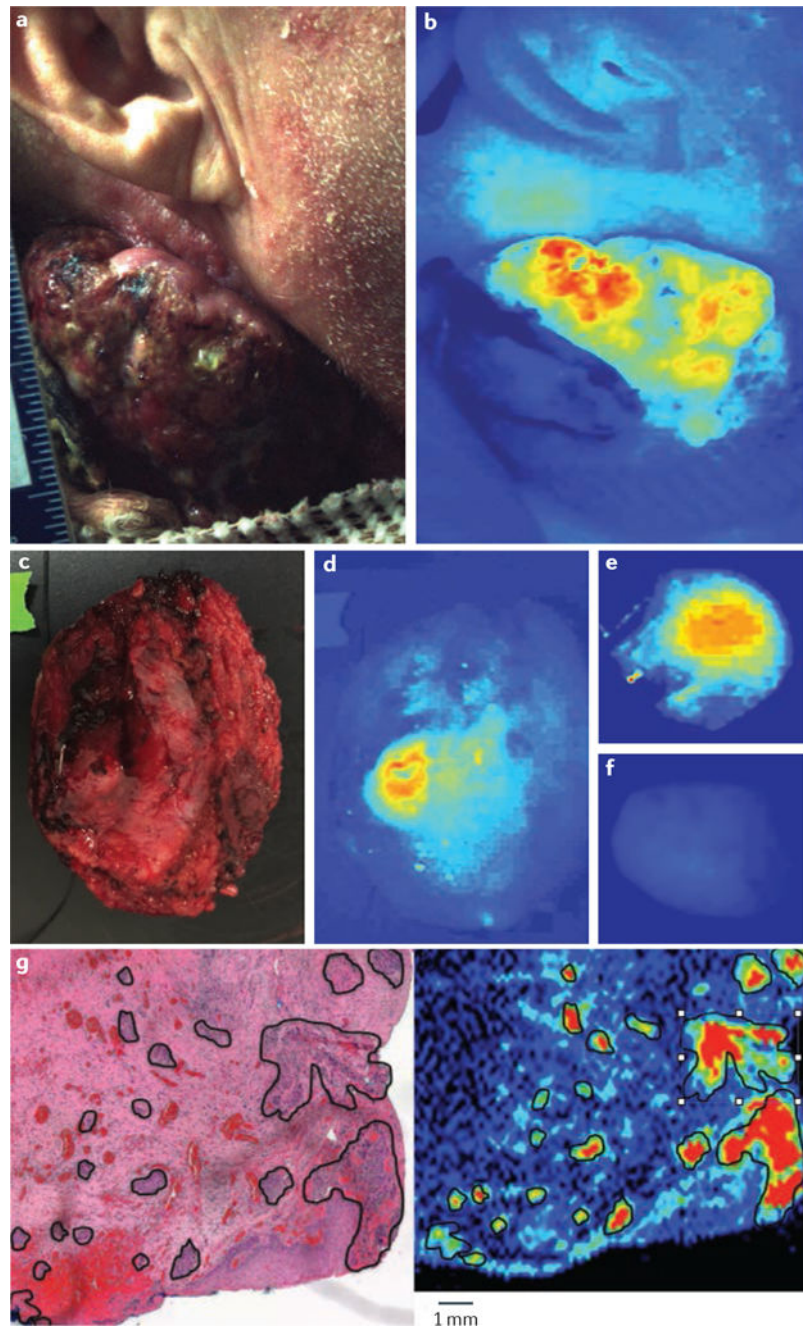
Figure 3. Cetuximab-800CW fluorescence in a patient with EGFR-positive head and neck cancer
a | Preoperative bright-field image of a patient with a cutaneous squamous-cell carcinoma and **b** | preoperative fluorescence acquisition of the same tumour 3 days after the patient received intravenous cetuximab-800CW (50 mg) (NCT01987375). The image was acquired using an open-field fluorescence imaging device (Luna; Novadaq, Ontario, Canada). **c** | A bright-field image of the deep surface of a resected cutaneous squamous-cell carcinoma tumour from a different patient taken 3 days after cetuximab-800CW infusion (50 mg). **d** | Open-field fluorescence images (obtained with Luna, Novadaq) of the same tumour depicted in **c** shows areas of positive fluorescence. Additional resected specimen was taken from a

deeper location than that of the primary specimen; positive areas of fluorescence were detected on **e** | the superficial surface, but not on **f** | the deep surface of the additional resection margin. **g** | Haematoxylin and eosin staining of 5 μm sectioned tissue from a primary tumour resected from another patient with a cutaneous squamous-cell carcinoma tumour taken 3 days after intravenous administration of cetuximab-800CW (50 mg). The outlined areas denote presence of cancer (assessed by a board-certified pathologist). **h** | Fluorescence scan (Odyssey; Li-COR Biosciences, Lincoln, Nebraska, USA) of the adjacent cut section, with outlined areas displaying bright fluorescence intensity.
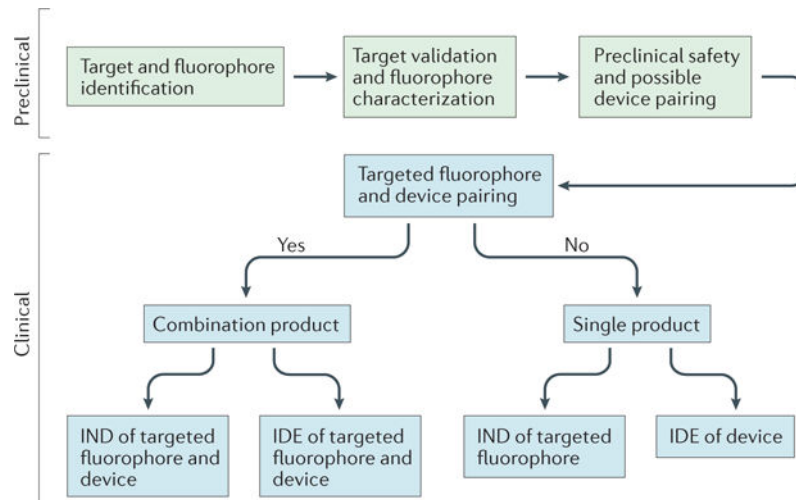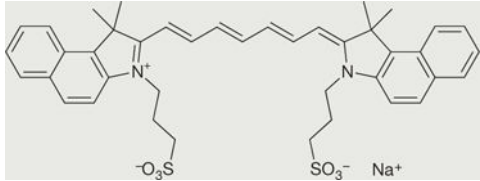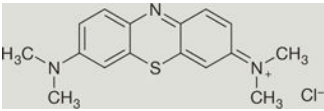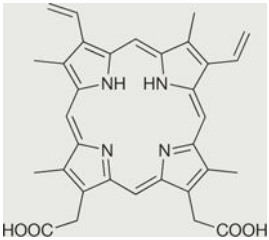
Figure 4. Preclinical and clinical development of targeted fluorophores
The preclinical development phase entails target identification and validation, and fluorophore characterization. The clinical development of targeted fluorophores can require pairing with a device optimized for that particular fluorophore or 'combination product'. IDE, investigational device exemptions; IND, investigational new drug.

Table 1
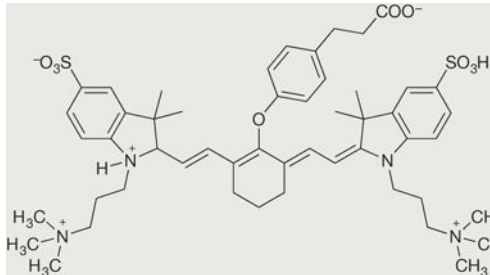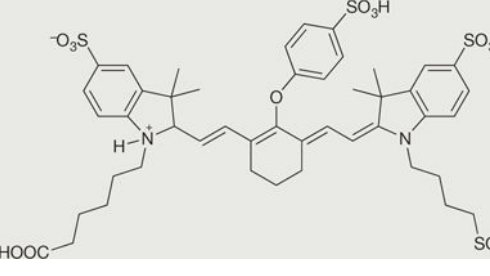
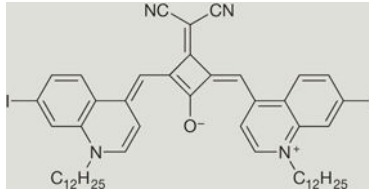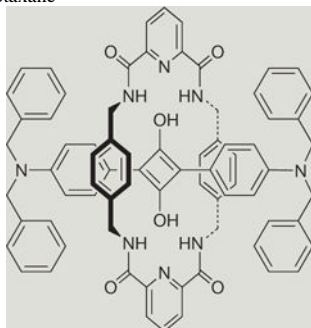Properties and uses of clinically approved fluorophores for cancer detection

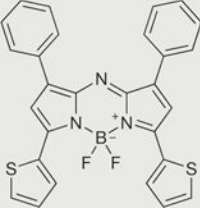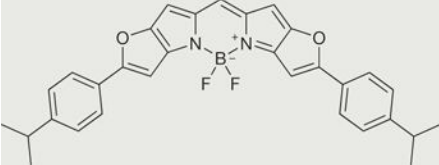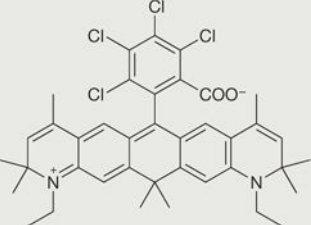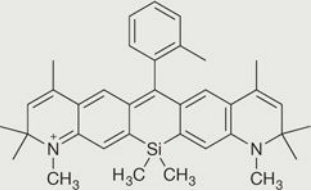| Fluorophore/range	Structure	Photophysical properties	Cancer indications*
Indocyanine green[29,37]/near-infrared		• λ_{ex}:807 nm • λ_{em}:822 nm • ε:121,000 $M^{-1} \times cm^{-1}$ • Φ:9.3% In FBS	• SLN mapping[21,40] • Hepatocellular carcinoma[50,51] • Liver metastases[49] • Other cancers[53–55]
Methylene blue[69]/far-red		• λ_{ex}:668 nm • λ_{em}:688 nm • ε:69,100 $M^{-1} \times cm^{-1}$ • Φ:4.4% In urine	• SLN mapping[28,40,47] • Fibrous pancreatic tumours[75] • Insulinomas[74] • Parathyroid adenomas[72] • Paragangliomas[30]
5-ALA (converted to PPIX)[134,173]/ visible		• λ_{ex}:405 nm • λ_{em}:635nm In ethanol	• High-grade gliomas[9,134] • Actinic keratosis[62,174,175] • Actinic basal-cell carcinoma[74,175–177] • Bowen's disease[59,62,174] • Squamous-cell carcinoma[62,178,179] • Other cancers[63,180]
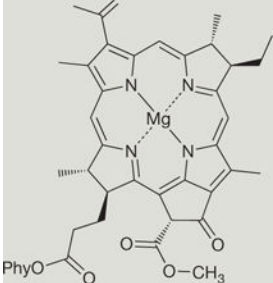
λ_{em}, emission wavelength; λ_{ex}, excitation wavelength; ε, molar absorptivity; Φ, fluorescence quantum yield; 5-ALA, 5-aminolevulinic acid; FBS, fetal bovine serum; PPIX, protoporfirin IX; SLN, sentinel lymph node.
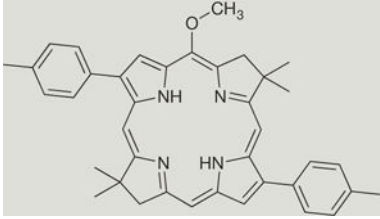
*
Tumour types refer to cancers in which fluorescence-guided surgery has been performed with these fluorophores.

Table 2

Fluorophores with NIR excitation and emission properties

Fluorophore class	Favourable characteristics	Limitations	Structures of representative NIR fluorophore analogues
Cyanine[19,37]	• Tunable fluorescence properties • Commercially available conjugates • Safety profile available for some fluorophores • Soluble in water	• Low quantum yield • Low photostability	ZW800⁻¹ IR800-CW
Squaraine[181,182]	• Intensely fluorescent • Narrow absorption bands • Conjugates available	• Low photostability in aqueous solution	Squaraine Squaraine rotaxane

Fluorophore class	Favourable characteristics		Limitations		Structures of representative NIR fluorophore analogues
BODIPY[183,184]	•	High extinction coefficient	•	Hydrophobicity	Aza-Bodipy
	•	High quantum yield	•	Small Stokes shift	
					Fused BODIPY (Keio Fluors)
Rhodamine[185,186]	•	Soluble in water	•	Lack of NIR fluorophores	10C-replaced rhodamine
					10Si-replaced rhodamine
Porphyrin and phthalocyanine[187,188]	•	Tunable fluorescence	•	Hydrophobicity	Bacteriopheophytin
			•	Aggregation in solution	
			•	Potential phototoxicity	
			•	Small Stokes shift	

Fluorophore class	Favourable characteristics	Limitations	Structures of representative NIR fluorophore analogues
			BChI-I

λ_{em}, emission wavelength; λ_{ex}, excitation wavelength; ϵ, molar absorptivity; Φ, fluorescence quantum yield; DCM, methylene chloride; FBS, fetal bovine serum; NIR, near-infrared; PBS, phosphate buffered saline.

Author Manuscript

Author Manuscript

Author Manuscript

Author Manuscript

Table 3

Clinical trials using targeted fluorophores for intraoperative cancer detection

Contrast agent	Ligand	Fluorophore	Target	Cancer type	Status/phase	Trial identifier
Antibody						
Bevadzumab-800CW	Bevacizumab	IR-800CW	VEGF	Breast cancer	I,II	NCT01508572 NCT02583568
				Colorectal cancer	I	NCT01691391
				Rectal cancer	I	NCT01972373
				Oesophageal cancer or dysplasia	I	NCT02129933
Cetuximab-800CW	Cetuximab	IR-800CW	EGFR	Head and neck cancer	I	NCT01987375
Panitumumab-800CW	Panitumumab	IR-800CW	EGFR	Head and neck cancer	IND	NCT02415881
ProstaFluor	huJ-591	IR-800CW	PSMA	Prostate cancer	IND	NCT01173146
MDX1201-A488	MDX1201	Alexa fluor 488	PSMA	Prostate cancer	IND	NCT02048150
Small peptide						
BLZ-100	Chlorotoxin peptide	ICG	Annexin A2	Soft-tissue sarcoma	I	NCT02464332
				Paediatric CNS tumours	I	NCT02462629
				Solid tumours	I	NCT02496065
				Adult glioma	I	NCT02234297
GE-137	MET ligand	Cy5	MET	Colon polyps and cancer	I	2010-019197-33
Activatables						
LUM015	GGRK peptide	Cy5	Cathepsin	Soft-tissue sarcoma, breast cancer	I	NCT01626066
AVB-620	Activatable cell-penetrating peptides	Cy5, Cy7	Proteases	Breast cancer	I	NCT02391194
Small molecule						
EI7	Folate	Fluorescein isothiocyanate	FR	Breast cancer	I	NCT01994369
				Lung cancer	I	NCT01778920
				Primary hyperparathyroidism	I	NCT01996072
				Renal-cell carcinoma	IND	NCT01778933
				Ovarian cancer	I	NCT02000778
OTL38	Folate	Cy7	FR	Ovarian cancer	II	NCT02317705

Contrast agent	Ligand	Fluorophore	Target	Cancer type	Status/phase	Trial identifier
				Renal-cell carcinoma	I	NCT02645409
				Pituitary adenomas	I	NCT02629549
				Neoplasms	I	NCT02602119
Multimodality						
Indium-111-DOTA-girentuximab-IRDye800CW	Girentuximab	IR-800CW	Carbonic anhydrase 9	Renal-cell carcinoma	I	NCT02497599

CNS, central nervous system; EGFR, epidermal growth factor receptor; FR, folate receptor; ICG, indocyanine green; IND, investigational new drug study; MET, hepatocyte growth factor receptor; PSMA, prostate-specific membrane antigen; VEGF, vascular endothelial growth factor.

Table 4

Instrumentation for fluorophore detection

Instrument	Fluorescence wavelengths (nm)	FDA/EMA status*	Applications	Manufacturer/commercial availability
Visible range				
SurgOptix T-3 platform[1,2,3]	520	Clinical trial (both)	OFS	SurgOptix, (Redwood Shores, California, USA)/NA
Multispectral fluorescence camera system[1,33,162]	520	Clinical trial (both)	• OFS • Fluorescein imaging	Technical University Munich and (Helmholtz Center Munich, Germany)/NA
Olympus[1]	Autofluorescence	Approved (both)	Endoscopic	Olympus Corp. (Tokyo, Japan)/Yes
Velscope[1]	Autofluorescence	Approved (both)	Endoscopic	Velscope (Atlanta, Georgia, USA)/Yes
Fluoptics[1,22]	520,670	NA	OFS	Fluoptics (Grenoble, France)/NA
Visible-to-NIR range				
ArteMIS[1,22,23]	400–1000	• Approved (both) • Clinical trial (FDA)	• OFS • Perfusion imaging • Detection of ICG and methylene blue	Quest Medical Imaging (Wieringerwerf, Netherlands and Akron, Ohio, USA)/Yes
NIR range				
SPY imaging system[1,21,22]	• λ_{ex}:806 • λ_{em}:820 • Centered: 830	Approved (both)	• OFS • ICG detection	Novadaq Technologies Inc. (Toronto, Ontario, Canada Inc.)/Yes
Photodynamic Eye (PDE)[1,21,22,165]	• λ_{ex}: 760 • λ_{em} >820	Approved/NA	• OFS • Handheld to detect ICG	Hamamatsu Photonics Co. (Hamamatsu, Japan)/Yes
da Vinci[1]	820	Approved (both)	Robotic	Intuitive Surgical (Sunnyvale, California, USA)/NA
PINPOINT[161]	820	Approved (both)	Endoscopic	Novadaq/Yes
Goggle system[22,188]	• λ_{ex}: 770 LEDs • λ_{em}: 830	Studies in animals/NA	• Wearable imaging of ICG • NIR-colour overlay	Y Liu et al.[186] (prototype Washington University, St. Louis, Missouri, USA)/NA

Instrument	Fluorescence wavelengths (nm)	FDA/EMA status*	Applications	Manufacturer/commercial availability
Fluobeam[21,22,23]	• λ_{ex}:750 • λ_{em}: >800	Clinical trial/NA	NA	Fluoptics/NA
mini-FLARE[53,160]	• λ_{ex}: 670, 689–725 • λ_{em}: 800–848	Clinical trial/NA	• ICG-assisted OFS • Methylene blue detection	Beth Israel Deaconess Medical Center (Boston, Massachusetts, USA)/Yes
PDE-neo/PDE-2 (REF. 164)	• λ_{ex}: 760 • λ_{em}: 820	Clinical trial/NA	• ICG-assisted laparoscopy	Hammamatsu Photonics Co. and Shinko Optical (Hamamatsu, Japan)/Yes
IMAGE1 SPIES[161,165]	• NA • White-light and ICG modes	Clinical trial (both)	• ICG-assisted laparoscopy • CW800-CA imaging	Karl Storz GmbH & CO. (Tuttlingen,Germany)/Yes
IC-View[21,41]	• λ_{ex}:780 • λ_{em}: NA	NA (both)	NA	Pulsion Medical Systems SE (Feldkirchen, Germany)/NA
Visual Navigator[21,46]	• λ_{ex}: 740 • λ_{em}: NA • Centred: 820	NA (both)	NA	SH System (Seoul, Republic of Korea)/NA
Leica FL800[21]	• λ_{ex}:700–800 • λ_{em}: 820–860	NA (both)	NA	Leica Microsystems Inc. (Buffalo Grove, Illinois, USA)/NA
INFRARED 800 (REF. 21)	• λ_{ex}:700–780 • λ_{em}: 820–900	NA (both)	NA	Zeiss Inc. (Jena, Germany)/NA
FIREFLY[21]	• λ_{ex}:806 • λ_{em}:NA	NA (both)	NA	Intuitive Surgical/NA
Laparoscopic NIR fluorescence system[21,32]	NA	NA (both)	NA	Olympus/NA

Instrument	Fluorescence wavelengths (nm)	FDA/EMA status*	Applications	Manufacturer/commercial availability
Prototype surgical navigation system[21]	• λ_{ex}: 760 • λ_{em}: 810–870	NA (both)	NA	Chinese Academy of Sciences/NA
GXMI Navigator[23]	• λ_{ex}:760 • λ_{em}: NA	Clinical trial/NA	• Intraoperative fluorescence imaging • ICG detection	Institute of Automation (Beijing, China)/NA
da Vinci Si system[163]	NA	NA (both)	Endoscopic ICG detection	Intuitive Surgical/NA
HyperEye[1,163,190,191]	• λ_{ex}:760–780 • λ_{em}:800–850	Experimental/NA	• Camera unit • ICG-assisted surgery	Mizuho Medical Co. (Tokyo, Japan)/Yes
Research use				
IVIS	• λ_{ex}: 415–760 (30 nm bandwidth) • λ_{em}: 490–850 (20 nm bandwidth)	Small-animal experiments (both)	• 3D tomography • Co-register to MR, CT, or PET-based imaging	Perkin Elmer (Waltham, Massachusetts, USA)/Yes
Maestro EX imaging system	500–950	Small animal experiments (both)	2D fluorescence imaging	Perkin Elmer/Yes
MiroSurge[192]	NA	NA (both)	Minimally invasive robotic surgery	NA
Lab-FLARE Model R1 open-space imaging system	• λ_{ex}: 400–660 (colour illumination), 665, 760 • λ_{em}: 400–650, 685–735, 781	NA (both)	Open-space imaging	Curadel Resvet Imaging (Marlborough, Massachusetts, USA)/Yes
Zeiss Pentero 900	560, 635, 820	Approved (both)	Microscopy	Zeiss Inc./NA
Leica OH5	635, 820	Approved (both)	Microscopy	Leica Microsystems Inc./NA

λ_{em}, emission wavelength; λ_{ex}, excitation wavelength; EMA, European Medicines Agency; ICG, indocyanine green; LED, light-emitting diode; NA, not applicable; NIR, near-infrared; OFS, open-field surgery.

*FDA-approved for clinical use but not for cancer detection.